

## **COPYRIGHT WARNING**

This paper is protected by copyright. You are advised to print or download **ONE COPY** of this paper for your own private reference, study and research purposes. You are prohibited having acts infringing upon copyright as stipulated in Laws and Regulations of Intellectual Property, including, but not limited to, appropriating, impersonating, publishing, distributing, modifying, altering, mutilating, distorting, reproducing, duplicating, displaying, communicating, disseminating, making derivative work, commercializing and converting to other forms the paper and/or any part of the paper. The acts could be done in actual life and/or via communication networks and by digital means without permission of copyright holders.

The users shall acknowledge and strictly respect to the copyright. The recitation must be reasonable and properly. If the users do not agree to all of these terms, do not use this paper. The users shall be responsible for legal issues if they make any copyright infringements. Failure to comply with this warning may expose you to:

- Disciplinary action by the Vietnamese-German University.
- Legal action for copyright infringement.
- Heavy legal penalties and consequences shall be applied by the competent authorities.

The Vietnamese-German University and the authors reserve all their intellectual property rights.





RUHR-UNIVERSITÄT BOCHUM



Vietnamese-German University



# HAPTIC STEERING UNIT WITH MAGNETORHEOLOGICAL BRAKE

BACHELOR THESIS

VGU, 2023



Vietnamese-German University

**Submitted by:** Vo Thanh Long

**RUB Student ID:** 108018207059

**VGU Student ID:** 13153

**Supervisor:** Prof. Dr. Nguyen Quoc Hung

**Co-supervisor:** MSc. Do Quy Duyen

DESIGNING A HAPTIC FEEDBACK STEERING SYSTEM USING  
MAGNETORHEOLOGICAL BRAKE

A BSc Thesis Presented

by

Võ Thành Long



Vietnamese-German University

Submitted to the department of Mechanical Engineering of the

RUHR-UNIVERSITÄT BOCHUM and VIETNAMESE-GERMAN  
UNIVERSITY

in partial fulfillment

of the requirement for the degree of

BACHELOR IN MECHANICAL ENGINEERING

January 2023

Major: Mechanical Engineering

## **AFFIRMATION IN LIEU OF OATH**

Võ Thành Long

Matriculation Number: 13153

I hereby declare in lieu of oath that I have produced the aforementioned thesis independently and without using any other means except the aids listed. Any thoughts directly or indirectly taken from somebody else's sources are made discernible as such.

To date, the thesis has not been submitted to any other board of examiners in the same or a similar format and has not been published yet.

Place, Date

Signature



## ABSTRACT

The electric power steering (ESP) system is currently being used commonly on vehicles in general and on the road in particular, but the benefits that ESP brings are not enough. Vehicles used in the working environment such as of marine, construction or off-road all need the most authentic driving feeling. And that is the main reason the haptic feedback steering system.

This thesis focuses on mechanical design a steering system model with haptic feedback by using magnetorheological fluid brake (MRB). More specifically, the procedure includes five main steps: analyzing the MRB types and optimizing the chosen one, selecting the significant components, and design the system.



## ACKNOWLEDGEMENT

I would like to express my sincere thanks to Pf. Dr. Hung Nguyen Quoc for guiding and helping me in completing my thesis on time. Similarly, I also want to offer my gratitude to the lecturers of the Mechanical engineering major in particular, Vietnamese-German University, and Ruhr-University in general.

Furthermore, I would like to show appreciation to Duyen Do Quy, a graduate of the Master's program at VGU and IU, for your help during the thesis work. Also, a special thanks to Tuu Nguyen Thi for her support during my study at the university.

Finally, I want to send my deepest thankfulness to my family and friends who have always encouraged me to overcome difficulties to complete the thesis.



# TABLE OF CONTENTS

AFFIRMATION IN LIEU OF OATH.....	1
ABSTRACT.....	2
ACKNOWLEDGEMENT .....	3
TABLE OF CONTENTS.....	4
LIST OF FIGURES .....	6
LIST OF TABLES.....	8
1. Introduction.....	10
1.1 Haptic feedback system overview.....	10
1.2 Problem and objective.....	10
2. Background theory.....	11
2.1 Haptic feedback.....	11
2.1.1 Haptic feedback definition .....	11
2.1.2 Haptic feedback system applications.....	12
2.2 Magnetorheological fluid (MRF).....	15
2.2.1 MRF overview.....	15
2.2.2 MRF characteristics.....	16
2.2.3 MRF applications .....	18
2.2.4 Choose the MRF.....	19
3. Design section.....	21
3.1 Configuration of MR haptic steering system .....	21
3.2 Design requirement .....	22
3.3 Design and select haptic feedback components .....	23
3.3.1 Select the MR brake type .....	23
3.3.2 Design the MR brake.....	36
3.3.3 Steering torque sensor .....	42
3.3.4 Position steering sensor .....	46
3.4 Design and select steering components.....	49
3.4.1 Shaft coupling.....	49
3.4.2 Pillar block bearing.....	49
3.4.3 Intermediate shaft .....	53
3.4.4 Steering wheel .....	53
3.4.5 Steering pedestal and transmission mechanism .....	54
3.5 Select power supply .....	56

4. Computer-aided design section.....	58
4.1 Assembly overview .....	58
4.1.1 MRB assembly .....	59
4.1.2 Rotation sensor unit assembly .....	60
4.1.3 Steering unit assembly.....	61
4.2 Component technical drawing .....	61
5. Conclusion and future work.....	74
5.1 Conclusion .....	74
5.2 Future work.....	74
REFERENCES .....	75
APPENDIX.....	78





## LIST OF FIGURES

Figure 1.1 LORD Tactile Feedback Device steering unit .....	10
Figure 2.1 The DIY haptic input knob.....	12
Figure 2.2 The “hRing” proposes a cutaneous sensation.....	13
Figure 2.3 Force feedback master-slave system .....	14
Figure 2.4 Conventional belt steering system.....	14
Figure 2.5 Basic modes of operation for MR fluid devices.....	17
Figure 2.6 Haptic knob using magnetorheological fluid .....	18
Figure 3.1 Haptic steering system operation diagram. ....	21
Figure 3.2 Haptic steering system configuration. ....	22
Figure 3.3 Sectional view of an original MR brake.....	23
Figure 3.4 Drum type MR brake.....	24
Figure 3.5 The magnetic field of drum type MRB using finite element analysis.....	25
Figure 3.6 Disc type MR brake.....	25
Figure 3.7 The magnetic field of disc type MRB using finite element analysis.....	26
Figure 3.8 The cross-sectional view of I-shaped MRB with width L and radius R .....	27
Figure 3.9 Structure of zigzag magnetic flux MRB.....	28
Figure 3.10 Zigzag magnetic flux.....	29
Figure 3.11 Tooth-shaped MRB structure .....	30
Figure 3.12 Simulated magnetic field lines around tooth-shaped MRB.....	30
Figure 3.13 Multiple-coil with the thin wall using finite element method .....	32
Figure 3.14 Steering column cover.....	34
Figure 3.15 Steering column cover dimension .....	34
Figure 3.16 I-shaped MRB components. ....	36
Figure 3.17 B-H curve of MRF-140CG.....	37
Figure 3.18 Offered MRB configuration. ....	37
Figure 3.19 MRB optimal results. ....	40
Figure 3.20 Structure of new I-shaped MRB.....	41
Figure 3.21 Eddy-current sensor.....	43
Figure 3.22 Eddy-current torque sensor .....	44
Figure 3.23 a) Torque sensor DR-3000 and b) its structure .....	45
Figure 3.24 Absolute encoder.....	46

Figure 3.25 Relative encoder .....	47
Figure 3.26 Encoder Omron E6B2-CWZ6C. ....	48
Figure 3.27 Flexible jaw coupling. ....	49
Figure 3.28 Pillow block ball bearing UCP 205 .....	52
Figure 3.29 UCP 205 technical specification provided by SKF.....	52
Figure 3.30 The angle of steering column in the drive cockpit. ....	54
Figure 3.31 Universal joint. ....	55
Figure 3.32 Timing pulley set with belt.....	55
Figure 3.33 Pulse power supply.....	56
Figure 3.34 Types of adjustable DC power supplies .....	57
Figure 3.35 Programmable DC power supply Keithley 2260B-80-13 .....	58
Figure 4.1 Exploded-view of MRB. ....	60
Figure 4.2 Rotation sensor unit.....	60
Figure 4.3 Exploded-view of steering unit. ....	61
Figure 4.4 Technical drawing of MRB components.....	62
Figure 4.5 Technical drawing of brake shaft. ....	63
Figure 4.6 Technical drawing of disc. ....	64
Figure 4.7 Technical drawing of inner case.....	65
Figure 4.8 Technical drawing of outer cover.....	66
Figure 4.9 Technical drawing of MRB holder.....	67
Figure 4.10 Technical drawing of bearing pillar base. ....	68
Figure 4.11 Technical drawing of intermediate shaft. ....	69
Figure 4.12 Technical drawing of encoder holder. ....	70
Figure 4.13 Technical drawing of steering column. ....	71
Figure 4.14 Technical drawing of steering pedestal. ....	72
Figure 4.15 Technical drawing of system base.....	73

## LIST OF TABLES

Table 1. General properties of magnetorheological fluids .....	16
Table 2. Comparison of selection for MRFs selection by LORD Corporation .....	19
Table 3. I-shape MRB parameter.....	28
Table 4. Zigzag magnetic flux MRB parameter. ....	29
Table 5. Tooth-shaped rotor MRB parameter.....	31
Table 6. Multiple coils with thin wall MRB parameter.....	32
Table 7. Hybrid MR brake general parameter table. ....	33
Table 8. Comparison of the three hybrid MRB types.....	35
Table 9. Colors corresponding to the output.....	48

## ABBREVIATION

MR:	Magnetorheological
MRF:	Magnetorheological Fluid
MRB:	Magnetorheological Brake
TFD:	Tactile Feedback Device
SUV:	Sport Utility Vehicle
EPS:	Electric Power Steering
VCC:	Voltage Common Collector
OV:	Output Voltage
GND:	Ground
LCD:	Liquid-crystal Display
TTL:	Transistor-Transistor-Logic
CPU:	Central Processing Unit
MIS:	Minimally Invasive Surgery



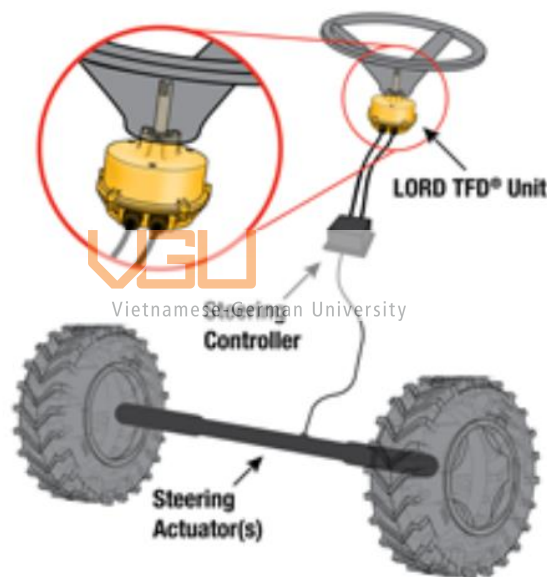
Vietnamese-German University

## 1. Introduction

Haptic technology was first introduced in the 1970s and its purpose was for the aircraft control surface [1]. Later on, a variety of haptic feedback systems have been made and innovated diversely in many forms.

### 1.1 Haptic feedback system overview

The concept of a haptic feedback steering system has been considered in recent years. Typical in this field is LORD Corp. who pioneers in development of a system similar to haptic feedback called the ‘Tactile Feedback Device’ (TFD) steering unit [2]. This system includes bearing support, steering position sensing, and communication assembled in one case. The signal is transmitted out by a cable to the steering controller.



*Figure 1.1 LORD Tactile Feedback Device steering unit [2].*

### 1.2 Problem and objective

Lord's ‘Tactile Feedback Device’ steering unit is for commerce, so the components are designed to be compatible with each other and difficult to replace. To change the maximum resistance torque feedback while driving, it is necessary to purchase a complete set, which is very expensive.

Therefore, this thesis aims to design a model of a haptic steering system for research purposes. In this system, the magnetorheological brake is one of the most important components for haptic feedback.

## 2. Background theory

### 2.1 Haptic feedback

#### 2.1.1 Haptic feedback definition

Haptic technology indicates any technology that involves the sense of touch by the user's experience through vibrations, motions, or forces [3]. Moreover, haptic feedback consists of methods in which the haptic technology communicates tactile information to users. Most of this haptic feedback can be categorized into two main classes: kinesthetic and tactile:

- ❖ **Tactile feedback** is the signal transmitted to the human brain when there is an interaction between human skin and the object's surface thanks to tiny receptors spread throughout the skin. On top of that, it comprises a sensation about the pattern, shape, and pressure.



Vietnamese-German University

Vibration can make a clear tactile feedback example. Some mobiles and tablets vibrate when the users interact with the touch screen to mimic the feeling of pressing a button or scrolling. Additionally, if the users switch the devices to silent mode, it will vibrate instead of a sound alarm when there is a call or a message.

- ❖ **Kinesthetic feedback** is proprioceptive information a person feels from sensors in tendons, muscles, and joint angles of arms, hands, wrists, and fingers. This feedback contributes to a person's perception of weight and resistance force.

A specific example of this kinesthetic feedback is a haptic input knob (Figure 2.1) that consists of a brushless DC motor with a hollow shaft for mechanically and electrically connecting the round LCD [4]. The motor is paired with an encoder to create torque feedback, which can be adjustable for a user to feel notches and detents. To sum up, users can feel mechanical resistance forces in their finger and wrist tendons while twisting a knob.



*Figure 2.1 The DIY haptic input knob [4].*

### **2.1.2 Haptic feedback system applications**

As technology becomes more and more advanced, the haptic feedback technology market is escalating aggressively. The worldwide haptic technology market size is expected to increase from 9,487 million USD in 2020 up to 25,240 million USD by 2027, which means it grows 1.66 times during 2021 – 2027 [5]. Some fields can benefit from haptic feedback:

#### **❖ Wearable haptic device**

Noticeable examples of wearable technology are “Samsung Galaxy Watch”, “Fitbit Versa”, and “NFC OPN Ring”. This market targets a key element which is interaction. Wearable haptics will allow gadgets to connect with the human wearer while they interact naturally with the surroundings. The wearable haptic devices vary not only do they provide vibration but also force sensations to all the fingers of the hands simultaneously.

In the Figure 2.2, the “hRing” includes two pairs of servo motors, a hook-and-loop fastener (Velcro support band), and a belt around the finger [6]. The actuation of the “hRing” is that one pair of motors spins in the opposite direction to create a normal force applying on the finger. And the second mode is the motor spin in the same

direction to produce the shear force. These modes are programmed to create the most realistic feeling when simulating the feeling of holding objects in space.

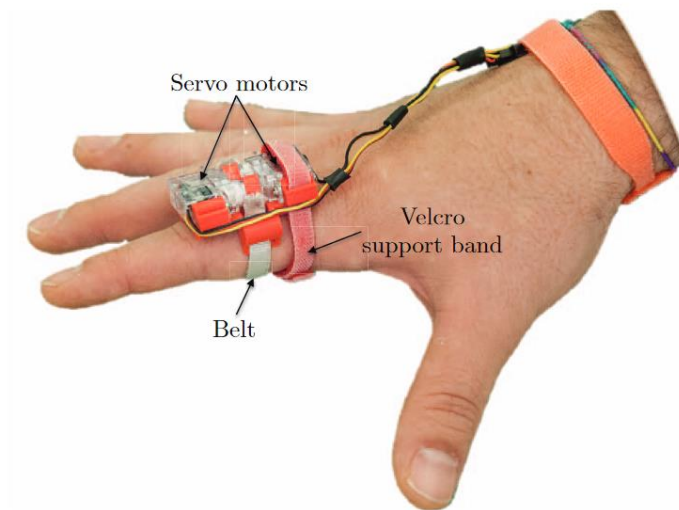


Figure 2.2 The “hRing” proposes a cutaneous sensation [6].

#### ❖ Controlling robot

Minimally invasive surgery (MIS) is a technique using advanced endoscopic tools with a slender camera through 3 or 4 small incisions. Though, it gives the surgeon an uncomfortable posture, tactile sensation, and uncertain coordination. As a result, a master-slave system using force feedback as the main signal is currently being trialed to resolve MIS limitations [7].

Figure 2.3 shows the excursion of a force feedback master-slave system in minimally invasive surgery. The control room (or haptic master M) in which the surgeon sits will send the control signal (C) to the main operating system, which is slave (S). Then, the Micro-slave is the surgical part that directly affects the patient, send haptic feedback in the form of vibration and resistance force back to the master. These feedbacks help the surgeon have a clearer perception of force as well as tactile sensation.



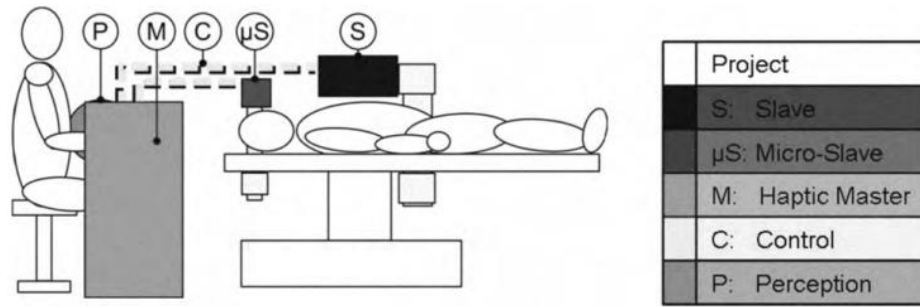


Figure 2.3 Force feedback master-slave system [7].

❖ **Stimulating steering system**

Video games, especially racing games, are one recognizable example of a haptic feedback steering system. A simulated racing steering (as shown in Figure 2.4) usually uses a gear system or a belt pulley in servo motors to stimulate the resistance force that a driving feeling brings upon the user.



Figure 2.4 Conventional belt steering system [8].

## 2.2 Magnetorheological fluid (MRF)

### 2.2.1 MRF overview

Magnetorheological fluid is classified as an intelligent material that can rapidly change state from liquid to nearly solid under an external magnetic field. This progress happens in a very short time (milliseconds). Additionally, the change in viscosity is continuous and reversible. For demonstration, the MR fluid can revert to a motion-free liquid after removing the magnetic field. This astonishing property makes MR fluid useful in mechanical systems requiring a simple, rapid-responded, and silent constitution for vibration and torque transmission.

The origin of the magnetorheological fluid was discovered by Jacob Rabinow at the US National Bureau of Standards in the 1940s based on the mechanism of the first invention which was a magnetic particle clutch [9]. The magnetic particle specialized iron powder is carried in a chamber. When no current voltage is applied, particles stay initially in powder form. But, when current runs through the coils, the created magnetic flux binds the particles together along the lines of flux. The magnetic field tightens the particles' bonding as the voltage-current rises, generating drag between the input and output when the clutch rotor cage passes through the particles. Therefore, torque can easily be controlled by the current.

Magnetorheological suspensions called intelligent material have rheological characteristics that fundamentally vary in response to a magnetic field. Ferrofluids and magnetorheological fluids (MRF) are two categories of these suspensions [10]. MR fluid is different from ferrofluid for its micrometer-scale particles while ferrofluid particles are primarily nanoparticles. MR fluid consists of three major components: magnetic suspension particles, a carrying fluid, and a stabilizer. The magnetic particles have a spherical shape with a diameter size ranging from 1 to 10  $\mu\text{m}$ . [11]. Carbonyl iron can be manufactured by disintegrating purified iron pentacarbonyl  $\text{Fe}(\text{CO})_5$ . The next component is the carrying fluid which is primarily chosen by the viscosity and temperature stability. Some common carrying fluids that can be listed are kerosene, synthetic oil, and silicon oil. Last but not least, the final component is the additive which is responsible for stabilizing the particles in the fluid. MRFs have two types of constancy: deposition constancy and conglomerate constancy. Deposition constancy

prevents the magnetic particles from subsiding after some time, while conglomerate stability guarantees the particles do not stick together. Some gels are demonstrated to meet these requirements. For a particular deposition example, a silica gel having a large surface area (100-300 m<sup>2</sup>/g) can hold the particles uniformly in the carrying fluid. On the other hand, ionic surfactants like oleic acid are utilized for the constancy of conglomerates.

## 2.2.2 MRF characteristics

### ❖ General properties

The main characteristics of MR fluids are summarized in Table 1. The initial state of viscosity for MR fluid is generally in the range of 0.1 to 0.3 Pa-s at 25°C. The most useful advantage of MR fluid is the response time. According to the magnetic circuit's architecture, this time ranges between 7 and 15 milliseconds. Under magnetic fields of 140-230 kA/m, the MR fluid can be demonstrated to yield stress up to 100kPa. Another advantage of MR fluid is that one can use permanent magnets to activate it without solid-state maintaining power requirements.



Vietnamese-German University

Table 1. General properties of magnetorheological fluids [10].

Properties	Value range
Initial viscosity	0.1-0.3 [Pa-s] (at 25 °C)
Density	21-32 [lb/gal]
Typical magnetic range	-1.5 to 1.5 [kAmp/m] -700 to 700 [Tesla]
Reaction yield stress range	5-70 [kPa]
Reaction time	Few milliseconds
Working current range	0-1.5 [A]
Work temperature	-40 to 130 [°C]

### ❖ Operational modes

Because MR is a smart fluid and is very sensitive to magnetic fields, it does not depend on external forces as well as the direction of the field lines. The change of axis and direction between the interacting parts and with the fluid creates three different working modes: valve mode, shear mode, and squeeze mode (Figure 2.5).

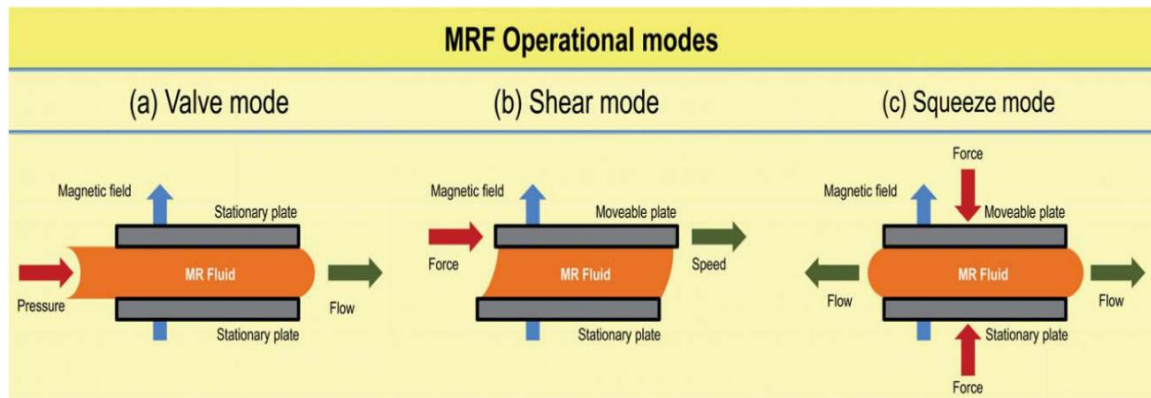


Figure 2.5 Basic modes of operation for MR fluid devices [12].

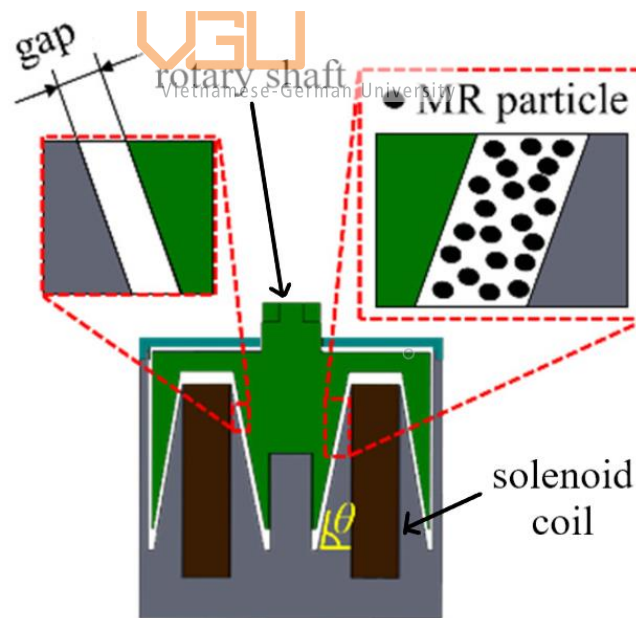
### ❖ Limitations

- **The price** of MR fluid is expensive (~ 216.39 USD / 500ml) [13].
- **The clumping effect** appears when the chain structure of particles lets the carried fluid flow freely. This is a result of letting the MR fluid under a very high magnetic field for a long time [14]. Additionally, the iron particles become fixed in place along the magnetic field lines while clumping, which distinguishes them from agglomeration. Although, the carrying fluid moves freely leaving the stuck particles.
- **Formation of agglomeration** is a defect in MR fluid caused by the conglomeration of iron particles and magnetization remnants. This agglomeration remains even after shutting down the magnetic field, causing a strong Van der Waal bond in the chain structure [10].
- **Temperature** affects MR fluids causing the variation in viscosity. The active temperature range for MR fluids is around -50 to 150°C [15].

- **Unstable pressure-driven flow** was expected to occur due to instabilities increasing when the MR flow is pressure driven. In research, the MR fluids flow through a tube under a non-uniform magnetic field. The result is that at a certain speed, part of the flow becomes unstable and its speed decreases. The flow showed a variety of tendencies, which may be attributed to the competing effects of hydrodynamic dissipation and the contact between the accumulates and the tube walls.

### 2.2.3 MRF applications

Choi et al. (2020) proposed a haptic knob that uses MR fluid [16]. Figure 2.6 shows how the haptic MR knob works quite similar to the MR brake. When there is current flowing in the solenoid coil, the viscosity of MR fluid in the gap will increase very quickly for a short period of time creating a resistance force acting on the rotary shaft. To sum up, users can feel mechanical resistance forces in their fingers and wrist tendons while twisting a knob.



*Figure 2.6 Haptic knob using magnetorheological fluid [16].*

Additionally, MRF is also used in shock absorbers or damper systems of the car industry. Among them, Chevrolet Corvette, Ford Shelby, etc., are currently equipped with this MR technology.

### 2.2.4 Choose the MRF

Because a magnetic field is produced in the radial direction, only the MRF at the outer side edge of the drum is activated in the drum-type brake. Different types of MRFs which are MRF-140CG, MRF-140BC, MRF-132DG, MRF-126LF, and MRF-122EG have been studied as shown in the following table.

Table 2. Comparison of selection for MRFs selection by LORD Corporation [17].

Properties	MRF-122EG	MRF-126LF	MRF-132DG	MRF-140CG	MRF-140BC
Appearance	Dark gray liquid	Dark gray liquid	Dark gray liquid	Dark gray liquid	Dark gray liquid
Viscosity (Pa-s) at 40°C	0.042 ±0.020	0.070 ±0.020	0.112 ±0.020	0.280 ±0.070	0.1140 ±0.040
Density (lb/gal)	29.50-31.20	22.03-23.70	24.60-26.30	29.50-31.20	31.30-32.96
Solid content by weight (%)	72	78	80.98	85.44	86
Operating Temperature (°C)	-40 to +130	-40 to +130	-40 to +130	-40 to +130	-40 to +130
Flash Point (°C)	> 150	> 150	> 150	> 150	> 150

From Table 2, it can be seen that MRF-122DG and MRF-126LF both have the smallest viscosity and friction force to operate with a 20 Nm torque requirement. On the other hand, the MRF-132DG can commonly be found in many brakes because of its index are more uniform than others. Prominently, Hamdan et al. (2014) pointed out that MRF-

140CG had a highest value of the magnetic field strength. Moreover, MRF-140CG has the smaller density and solid content by weight than MRF-140BC, which makes its formation of agglomeration and clumping effect happens less. Additionally, with a small amount of MRF-140CG, then the brake has enough braking torque because magnetic field strength is proportional to the magnitude of torque.

In a word, the MRF-140DG is chosen as the most appropriate for this haptic steering system. According to LORD Corporation, MRF-140DG owns some features and benefits:

- **Dynamic yield strength:** because of an average viscosity index, it has relatively high yield strength in the absence of the magnetic field. As a result, it provides an efficient yield strength in a magnetic field; allowing a flexible control ability.
- **Temperature resistant:** works stably in a wide temperature range and meets the performance demands.
- **Non-abrasive:** formulated to not abrade the devices using the MR fluid.
- **Fast response time:** response to changes in the magnetic field and reverse into initial form instantly.
- **Deposition resistant:** provides high resistance to deposition, and easy to replace.



Vietnamese-German University

### 3. Design section

#### 3.1 Configuration of MR haptic steering system

##### ❖ System overview

The haptic steering system works like a closed-loop control system (Figure 3.1). Input is the desired resistance force of the MR brake. The central processing unit (CPU) is responsible for controlling the haptic feedback steering system by managing programmable DC power supply output. This supplied output current determines the resistance torque of the MR brake. System output is the torque generated by the MR brake against the driver's steering torque. Simultaneously, the CPU also presents by a display monitor to easily observe the operation of the system. The rest is the torque sensor, and encoder whose job is to provide a measured output of torque, and steering rotation position to the control unit, respectively. When the torque output has reached the required maximum value, the CPU will stop the system. The main purpose is to prevent overload causing MR brake damage.

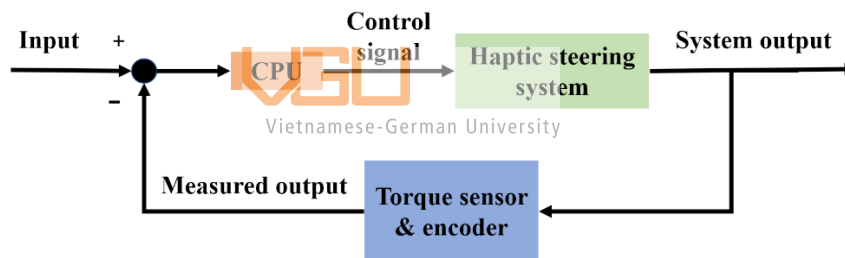


Figure 3.1 Haptic steering system operation diagram.

##### ❖ Configuration

The configuration of the haptic steering system consists of the following main components: a steering wheel, an encoder, a torque sensor, and an MRB. These components are held fixedly on a base plate by pedestals. Their shafts are connected by couplings. The arrangement of the position of each part is shown in Figure 3.2 below. The power supply and CPU circuitry are on the outside. They connect to the system through signal wires and electric wires.



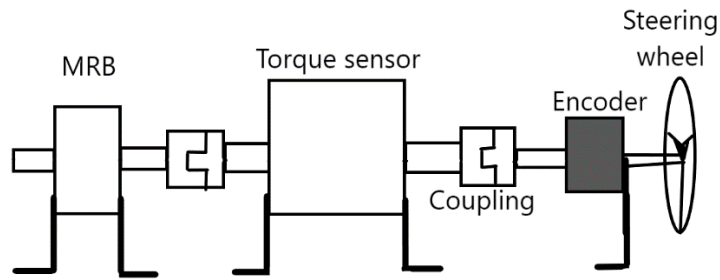


Figure 3.2 Haptic steering system configuration.

### 3.2 Design requirement

#### ❖ Resistance torque

The hypothesis is that with a car steering wheel has a diameter of 34cm, there is a torque that prevents the driver from turning the steering wheel. In addition, this torque has a magnitude of 20Nm. Based on the formula for calculating torque:

$$\tau = F \times d \quad (1)$$

With  $\tau$  is the torque [Nm]

F is the extended force [N]

d is the distance (diameter in this case) [m]

The resistance force appearing at the steering wheel is 58.8N equivalent to 5.9kg. If the driver wants to continue turning the wheel, that person must use their strength to overcome the resistance force. For an adult, turning the steering wheel with a force of 6kg is enough to feel heavy, and knows it is the limit that the steering wheel cannot rotate anymore. In closing, the hypothesis is valid, so the MR brake is responsible for creating the highest resistance torque of 20Nm.

#### ❖ Off-stated torque

There is a requirement that when the MR brake is in an inactive state (off state), the steering wheel can rotate smoothly. But the viscosity of MRF still remains causing of resistance torque. Therefore, the MR brake must be designed so that the resistance torque is as small as possible. In this case, the resistance torque equals 0.2Nm is acceptable.

### ❖ Working space

There are no specific requirements. Since the system model works in the laboratory, the haptic steering system should not be too cumbersome for ease of assembly or movement. In conclude, the operating space of the system should be limited in  $1\text{m}^3$  space.

## 3.3 Design and select haptic feedback components

### 3.3.1 Select the MR brake type

#### 3.3.1.1 MR brake types analysis

The physics mechanism of MR brakes is inherited from almost all characteristics that different brake types own. Most of the brakes on the market use friction on both sides of the wheel. The collective wheel pressing converts kinetic energy into heat energy. As can be seen in Figure 3.1, the magnetorheological fluid (MR fluid) acts as a brake pad, clamping on the brake disc (also known as the rotor) and slowing the shaft down. More specifically, this fluid blocks the rotation by its viscosity which is greatly increased under a magnetic field when there is an electric current flowing through the coil.

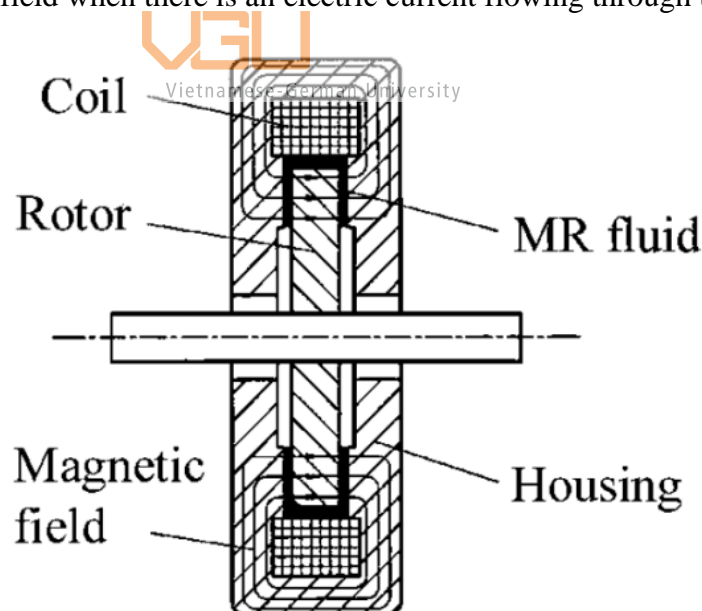


Figure 3.3 Sectional view of an original MR brake [9].

### ❖ Drum type

The venerable drum brake is still used by some of today's vehicles because it offers a reasonable price. But it getting less and less every year due to the time-consuming maintenance.

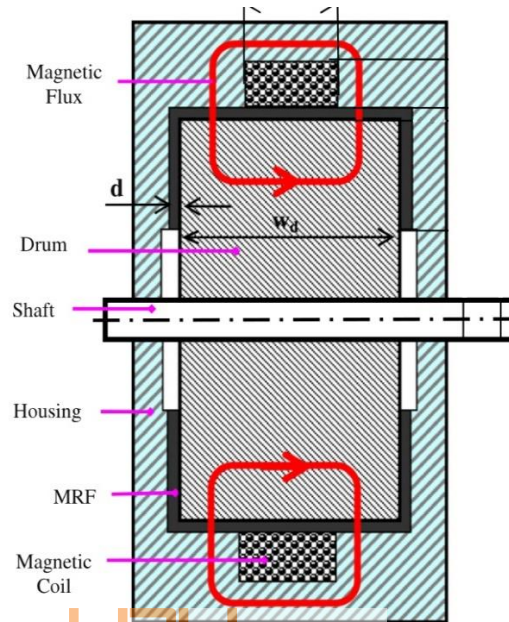


Figure 3.4 Drum type MR brake [18].

### ❖ Drum and inverted drum type

#### Advantages

- It produces less heat because the vehicle's front brakes produce the majority of the stopping power.
- In comparison to disc brakes, it emits or produces less particulate matter.
- Because the resistive contact area is at the circulative surface, it provides a higher drag force than a disc brake of a similar diameter.
- It required less maintenance than the disc to increase corrosion resistance.
- It is trustworthy and less expensive.

#### Disadvantages

- Heavy braking can result in excessive heating, which can then distort the drum and cause a vibration when braking.
- During hard braking, the drum's diameter slightly grows as a result of thermal expansion.

- It is possible for MR fluid degradation from overheating.
- The brake fluid may be heavily damaged if the brake drums are heated excessively.

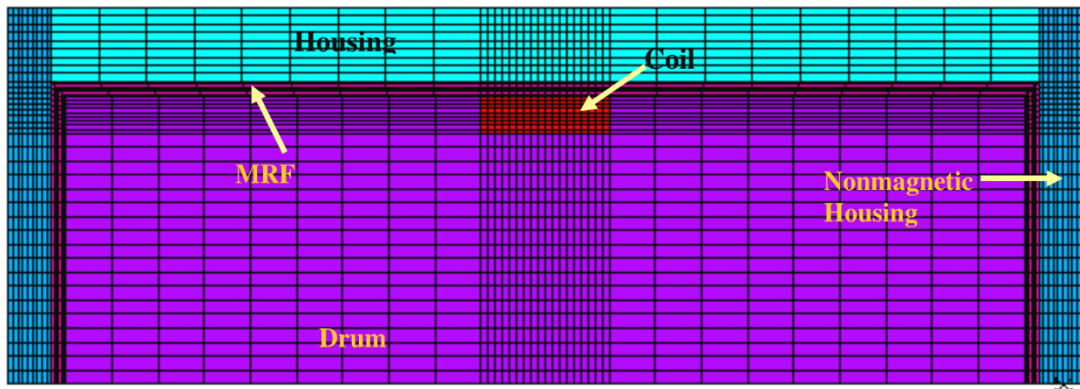


Figure 3.5 The magnetic field of drum type MRB using finite element analysis [18].

#### ❖ Disc type

This type of brake is well-known for its simple structure and ease to assemble the components. Above that, the disc-type MRB builds a basic vital fundamental in the innovation process. Many different types of MRBs in the new generation are learned from this disc brake meeting the higher demands upon the braking torque, and mass.

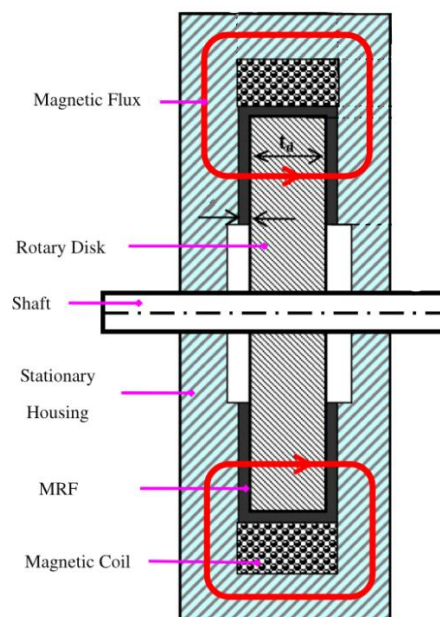


Figure 3.6 Disc type MR brake [19].

## Advantages

- In contrast to drum brakes, disk brakes take less effort (brake torque) to stop.
- Compared to drum brakes, it produces less heat while providing the same amount of braking torque.
- Since the disk brake is independent of the wheel rim, maintenance is simple.
- It is less prone to slide when wet (when applied with caution) compared to the drum brake.
- When braking force is applied forcefully, it is safer than drum brakes.
- Because of the smaller friction surface area, a disc brake cools down more quickly.

## Disadvantages

- It is expensive.
- It might be troublesome if there is any air left in the disk braking system since the brakes could not function properly.
- Drum brakes are simpler than disk brake assemblies, which have more moving components.

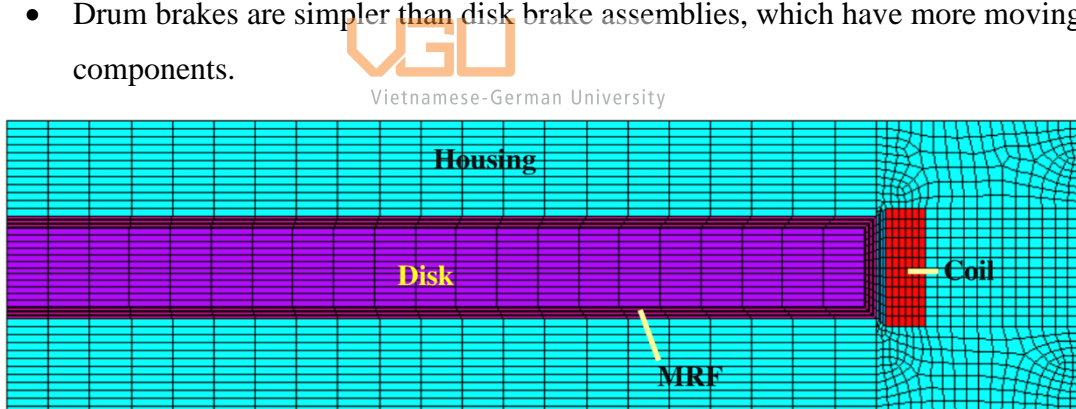


Figure 3.7 The magnetic field of disc type MRB using finite element analysis [19].

## ❖ Hybrid types

Beginning with the initial idea to design a brake using MRF, a disc-type MRB was invented. The disc type MRB includes a magnetic coil wrapped outside the cylindrical disc. MRF is inserted in the gap between the coil and the disc. This simple structure makes the disc-type MRB easy to manufacture and stimulate. Nonetheless, there still is a flaw in this type called “bottleneck” which hinders the performance of the brake. On the other hand, the disc type is not suitable when it comes to a working place with a

long cylinder shape. Then a drum-type MRB is a more reasonable one. Compare to the disc type, the drum type's mass is greatly higher while both of their maximum demand torques are equal. Additionally, Nguyen Q H et al. introduced a new type of MRB which has coils outside of the housing and thin walls divided between each coil in multiple coils case. This type of MRB can reduce the bottleneck problem. In recent years, there is an amount of research on innovating the MRB by creating many complex different shape types. These modern MRB can be mentioned as I-shaped, tooth-shaped, and zigzag magnetic flux MRBs. Some studies show that these hybrids not only decrease the bottleneck issue significantly but also gain a high braking torque with such a small amount of mass.

- **MRB with I-shaped rotor**

Bien et al. (2022) proposed a complex shape MR brake that obtains not only compacity but also guarantees the demanded braking torque [20]. The solution is to design an I-shaped MR brake based on the MR disc-type brake. With the “I” shape, this MR brake provides a large contact area between the MRF and the braking rotor, which creates a higher magnetic flux that leads to higher torque.

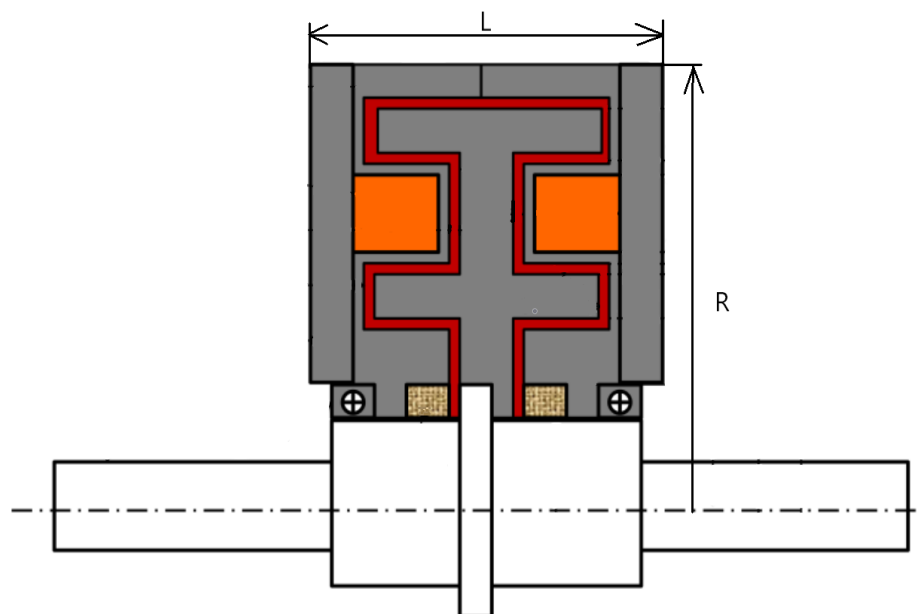


Figure 3.8 The cross-sectional view of I-shaped MRB with width  $L$  and radius  $R$  [20].

According to Bien et al. (2022), the optimal parameter is calculated by ANSYS APDL using the integration method. The optimal setup is the braking torque equal to 20Nm, the stainless (SS304) steel is used for the non-magnetic parts, and MRF-132DG is filled in the gap. The 24-gage copper wire is the element of the coil. The result can be observed in the table.

Table 3. I-shape MRB parameter

Braking torque [Nm]		Dimension [mm]		Mass [kg]	Power consumption [W]
Max.	Off-state	L	R	2.21	73.7
19.9	0.21	36.0	50.0		

- **MR Brake with zigzag magnetic flux path**

Based on the disc type MR Brake, Hung Ng. (2021) offered a new MRB descendant that inherits the uncomplicated assembly of disc-type MRB and gains a strong magnetic field between zigzag-positioned plates [21].

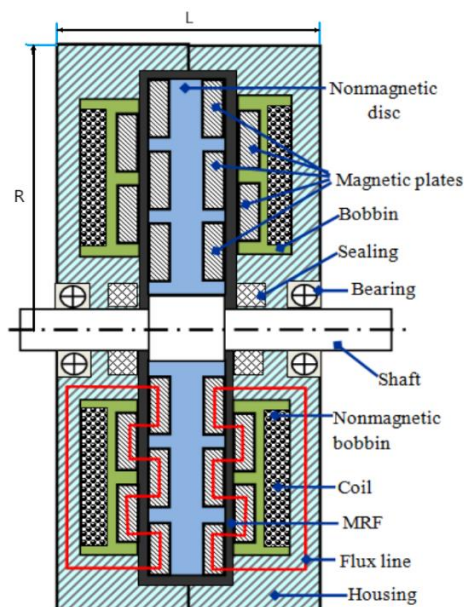


Figure 3.9 Structure of zigzag magnetic flux MRB [21].

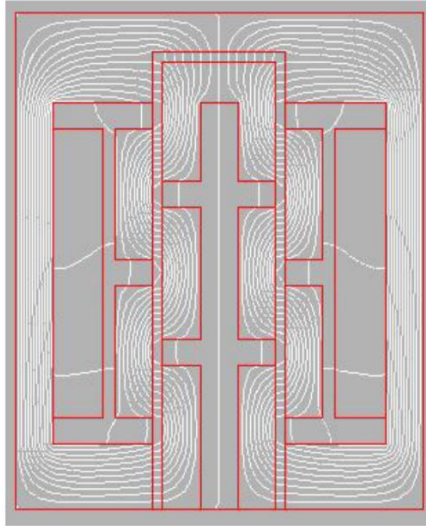


Figure 3.10 Zigzag magnetic flux [21].

The maximum braking torque is set 20Nm. The configuration is a 24-gage coil wire working with a 2.5A current. From the testing, the 2.5A current is an important condition to achieve a maximum torque 20Nm. Another notice is that the bobbin is made of 1350 aluminum alloy.

Vietnamese-German University

Table 4. Zigzag magnetic flux MRB parameter.

Braking torque [Nm]		Dimension [mm]		Mass [kg]	Power consumption [W]
Max.	Off- state	L	R	2.35	80
20.01	0.20	22.0	67.0		

- **MR Brake with tooth-shaped rotor**

There are many research studies about how to improve an MRB for practical applications or industrial use. The main purpose is to get higher braking torque, volume and mass mobility, and minimum power consumption. The large contact area filled up with the MRF is the key to producing high braking torque but also



keeps the volume of the MRB compact. Gotten this idea, Nguyen et al. (2018) offered the MRB with a tooth-shaped cross-section of the rotor [22]. The mechanism of this tooth-shaped MRB is that each tooth works as a magnetic pole. Two magnetic coils are placed on both sides of the brake, generating the magnetic field. The inner housing also has a tooth-shaped to match the rotary disc. The MRF fills in the gap between the inner housing and the disc.

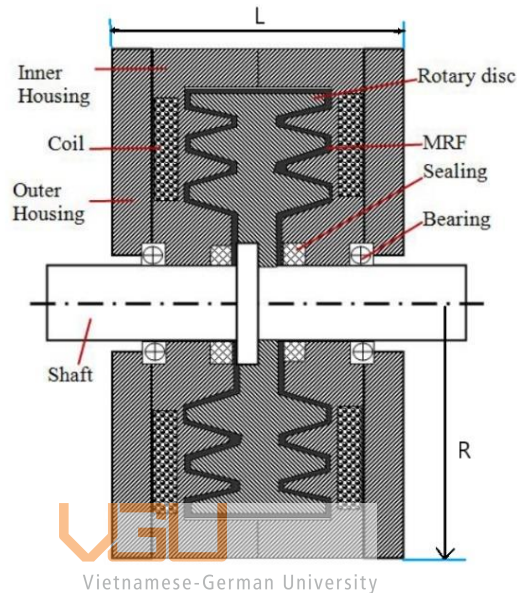


Figure 3.11 Tooth-shaped MRB structure [22].

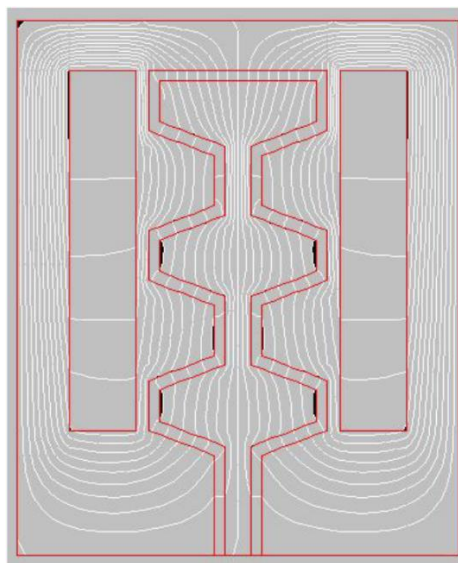


Figure 3.12 Simulated magnetic field lines around tooth-shaped MRB [22].

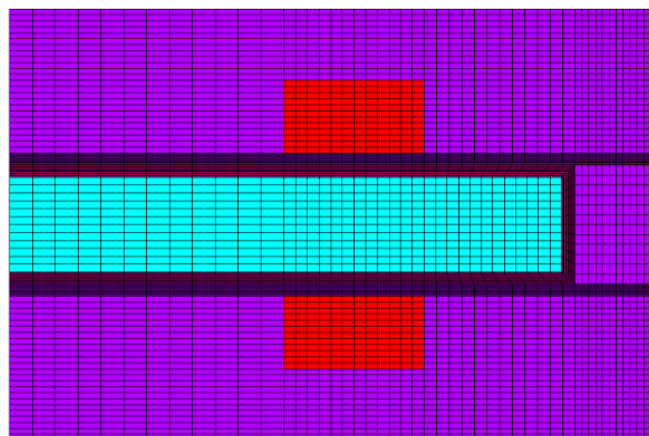
The configuration for maximum torque 20Nm of the tooth-shaped rotor is a 24-gage wire coil with a working current of 2.5A and the material for MRB is steel C45. The testing applies the MRF132-DG.

Table 5. Tooth-shaped rotor MRB parameter.

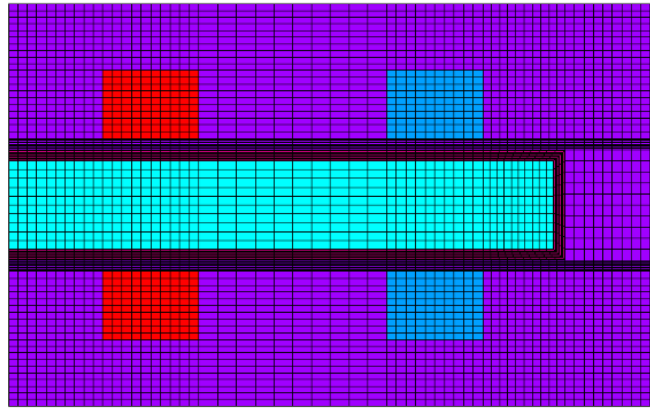
Braking torque [Nm]		Dimension [mm]		Mass [kg]	Power consumption [W]
Max.	Off- state	L	R	1.32	64.58
19.893	0.24	68.0	54.8		

- **MR Brake using multiple side-coil with thin wall**

Nguyen Q H et al. (2021) offered a new design to optimize manufacturing and improve the performance of the MRB [23]. The coils in this proposed MRB are mounted directly on the inner surface of the MRB's side housing and are kept apart from the operating MR fluid by a thin wall.



a)



b)

Figure 3.13 Multiple-coil with the thin wall using finite element method [23].

a) Single coil and b) Double coil

Table 6. Multiple coils with thin wall MRB parameter.

Coil quantity	Braking torque [Nm]		Dimension [mm]		Mass [kg]	Power consumption [W]
	Max.	Off-state	L	R		
Single coil	20.0	0.22	22.0	63.0	2.8	37.3
Double coil	20.0	0.21	19.0	67.0	2.3	58.5

❖ **Conclusion:**

Only the MRF on the end face of the disc is magnetized in the case of disc brakes. Because a magnetic field is generated in the radial direction, only the MR fluid on the outer edge of the drum is activated in a drum type brake. Both disc type and drum type have pros and cons. The solution for such cases is to take into account the combination of disc type and drum type. In conclusion, hybrid type MR brake is the most effective and optimal choice. Then, the parameters of the hybrid type MRB are summarized in the Table 7 below.

Table 7. Hybrid MR brake general parameter table.

Parameter		Type	I-shaped	Tooth-shaped	Zigzag magnetic flux
		Dimension [mm]	L	36.0	68.0
	R	50.0	54.8	67.0	
Mass [kg]			2.21	1.32	2.35
Power [W]			73.7	64.58	80.0
Torque [Nm]	Max		19.9	19.893	20.01
	Off-state		0.21	0.24	0.20

### 3.3.1.2 MR brake evaluation criteria

- **Dimension**

The initial aspect that needs to be scrutinized first is the brake's shape and dimension. The dimension of the brake depends on the car's steering column cover. The intended target is the sport utility vehicle (SUV) which has strong mobility on steep passes and many other types of terrain - a feature that can be understood as off-road. Almost every SUV itself owns an electric power steering system because of some comfortable assist features. The EPS can change the wheel direction without steering torque from the driver. This is a convenience but also a drawback. Drivers who prefer a "traditional" manual transmission car usually complain about the ESP system not bringing the practical drive feeling, especially in off-road cases. When driving on zigzag and cambered roads, the steering feels too light-weight while the wheels are suffered from intensive shaking inconsistently.

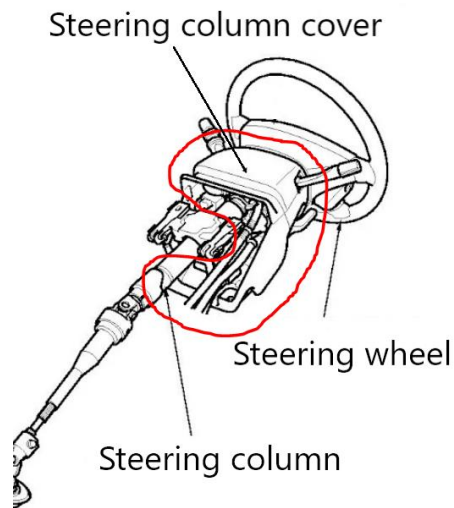


Figure 3.14 Steering column cover [24].



Figure 3.15 Steering column cover dimension [25].

The MR brake needs a diameter or width maximum limit of 282.575mm to fit in the steering column cover. The best optional choice for drivers to have a comfortable space is the brake outer diameter must be below 250mm. Moreover, the geometry dimension will be considered as small as possible for the compact characteristic.

- **Mass**  
The mass aspect is considered for installing and delivering the steer-by-wire tactile prototype.
- **Power consumption**  
With the approximately equal provided torque, the MR brake with the smallest power consumption will be appreciated. Because the power consumption directly involves the heat emitting, leads to an increase in entropy. By the same result that creates 20Nm torque, the more power is consumed, the more unusable energy is released.
- **Working temperature**  
The temperature when the MRB is working affects the durability as well as longevity of the tactile steering system.
- **Structure simplicity**  
The structure simplicity shows whether the MRB is easy to manufacture or not.

Table 8. Comparison of the three hybrid MRB types.

From 1 to 5 corresponding from lowest to highest satisfaction point.

Types \ Aspect	I-shaped	Tooth-shaped	Zigzag magnetic flux
Dimension	4	3	3
Mass	3	5	2
Power consumption	3	3	2
Working temperature	4	4	3
Structure simplicity	5	3	5
<b>Total point</b>	<b>19</b>	<b>18</b>	<b>15</b>

### ❖ Conclusion:

In sum, I-shaped has the highest score from the table above. Therefore, this thesis proceeds to use an I-shaped MRB for the haptic steering system.

## 3.3.2 Design the MR brake

### 3.3.2.1 Configuration and principle of I-shaped MRB

The structure of an I-shaped MRB includes the main parts: housing inner part, outer cover, coil, disc, and MRF (Figure 3.16). Between the brake case and the rotary disc brake is a thin layer of the MRF. The magnetic coil is wrapped into the groove of the I-shape and protected by the outer cover. The magnetic field strength builds on the level of the provided current. To sum up, controlling the braking torque means adjusting the applied currents.

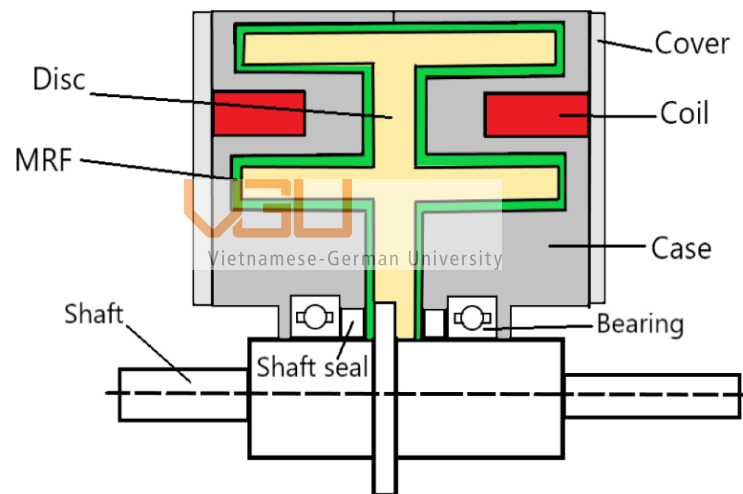


Figure 3.16 I-shaped MRB components.

### 3.3.2.1 Magnetic analysis of I-shape MRB

In this part, the MRB magnetic flux will be examined using the FEM approach. The magnetic fields are divided into subdivision in ANSYS APDL analysis. The quantity of subdivision per line affects the scale of the grid. As long as the border of the magnetic field is parallel, the outside faces of the non-magnetic cover are defined as the magnetic field's limit. The magnetic characteristics of components such as inner cases the disc, and the MRF inside are presented as a curve B-H.

The B-H magnetic properties of the MRF are determined by the following empirical equation:

$$B = 1.91\Phi^{1.133}[1 - \exp(-10.97\mu_0H)] + \mu_0H \quad (2)$$

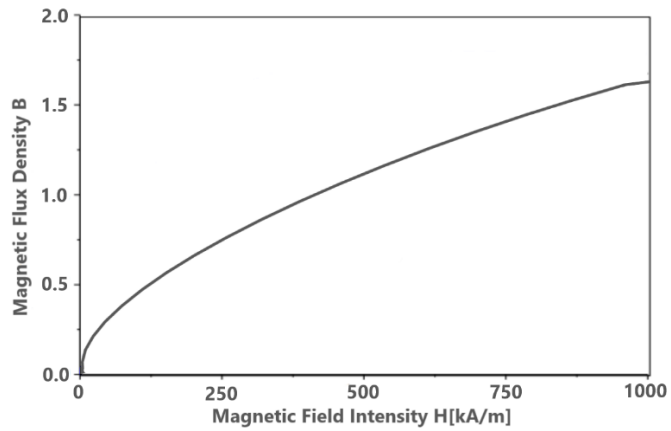


Figure 3.17 B-H curve of MRF-140CG.

### 3.3.2.2 Torque calculation

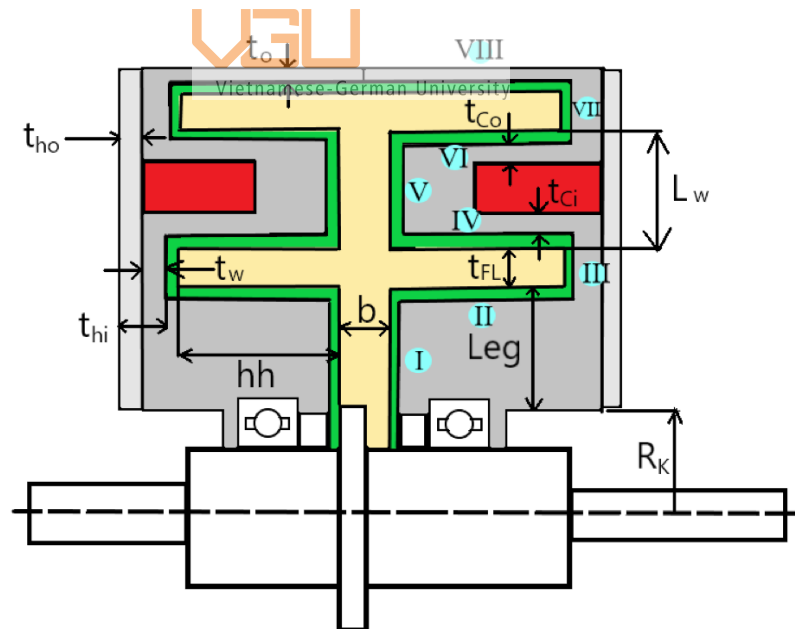


Figure 3.18 Offered MRB configuration.



Figure 3.18 divides areas for different braking torque. The total braking torque generated by the MRB is calculated by the following formula [20]:

$$T_B = 2 \times \left( \sum_I^{VIII} T_k + T_{ss} + T_{br} \right) \quad (3)$$

Where  $T_k$  is the braking torque that the MRF generates on the individual  $k^{\text{th}}$  part

$T_{ss}$  is the friction moment between the radial shaft seal and the shaft

$T_{br}$  is the bearing's friction torque

Area I, III, V, VII is symmetrical around a central axis, so their friction torque is determined by:

$$T_k = \frac{\pi \mu_k}{2d} \times [R_{k+1}^4 - R_k^4] \times \Omega + \frac{2\pi \tau_{yk}}{3} \times (R_{k+1}^3 - R_k^3) \quad (4)$$

with  $k$  are I, III, V, VII



Area II, IV, VI, VIII formed by annulus-shaped grooves. Because of that, they are defined as follows:

$$T_k = 2\pi R_k^2 \times l_k \times \left( \tau_{yk} + \mu_k \frac{\Omega R_k}{d} \right), \quad (5)$$

with  $k$  are II, IV, VI, VIII

Where  $R_k$  is the radius of the defined area in the MRB shown in Figure 3.18

$d$  is the gap thickness to fill in MRF

$\mu_k$  is average viscosity of MRF

$\tau_{yk}$  is the yield stress of MRF

$\mu_k$  and  $\tau_{yk}$  are the variables determined at the  $k^{\text{th}}$  areas. These are calculated to approximate the exact value through an equation described as follows:

$$\mu_k = \mu_\infty + (\mu_0 - \mu_\infty)(2e^{-B\alpha\mu_k} - e^{-2B\alpha\mu_k}) \text{ with } k = I \rightarrow VIII \quad (6)$$

$$\tau_{yk} = \tau_{y\infty} + (\tau_{y0} - \tau_{y\infty})(2e^{-B\alpha_{\tau k}} - e^{-2B\alpha_{\tau k}}) \text{ with } k = I \rightarrow VIII \quad (7)$$

Where  $\mu_0$  and  $\tau_{y0}$  are viscosity and yield stress respectively of MRF at field equal zero  
 $\mu_{\infty}$  and  $\tau_{y\infty}$  are viscosity and yield stress of MRF at saturation state  
 $\alpha_{\mu k}$  and  $\alpha_{\tau k}$  are the saturation moment index of the viscosity and the yield stress  
 $B$  is the induced magnetic density

Friction torque of the shaft seals can be approximately calculated by the analytical formula below:

$$T_{ss} = 0.65 \times (2R_{ss})^2 \times \omega^{\frac{1}{3}} \quad (8)$$

Where  $R_{ss}$  is the shaft diameter contact to the shaft seal [inches]  
 $\omega$  is the angular speed of the shaft [RPM]

Deep groove ball bearings are chosen for this study, and the frictional moment of these bearings may be calculated as follows:

$$T_{br} = \mu_{br} \times \frac{P \times d_p}{2} \quad (9)$$

Where  $\mu_{br}$  is the friction coefficient of gasoline ball bearing approximately 0.0015  
 $P$  is the corresponding load applying on the drive  
 $d_p$  is the pitch diameter of the bearing

### 3.3.2.3 Optimal MR brake design

The optimization aim is for the MRB to have the lightest mass possible, and the braking torque must also meet the requirements. Furthermore, its basic form has not changed significantly. The optimal shape is calculated using the formula:

$$m_B = V_d \rho_d + V_c \rho_c + V_{cs} \rho_{cs} + V_s \rho_s \quad (10)$$

With the requirement:  $T_{Bmax} \geq T_{rB}$

Where  $V_d, V_c, V_{cs}, V_s$  and  $\rho_d, \rho_c, \rho_{cs}, \rho_s$  are the volumes and mass densities of the brake disc, the coils, the case, and the rotating shaft respectively.

$T_{Bmax}$  is the MRB's maximum practicable braking torque

$T_{rB}$  is the required braking torque

And the required braking torque is set by 20Nm.

### ❖ Optimal result

In the optimization, design variables are defined for important MRB design variables such as: the inner groove radius (Ri), outer groove radius (Ro), case body length (Lc), brake shoe thickness (tSh), brake shoe height (hSh), the thickness of the cover and case (tcv and tcs). The coil bobbin has wall thicknesses (tcw, tw1, and tw2) and width (wc). It is noted that the MRF gap, whose manufacturing technique is taken into account, is practically confirmed to be 0.8mm. In this study, the optimization issue is solved using the first-order approach that is directly integrated into ANSYS APDL's optimization toolbox.

The ANSYS Workbench software generates a variety of configuration results. Then, the program will compare the index of the configurations and give the final result that is the most suitable for the requirements. Figure 3.19 shows that the 38th configuration is the most optimal result: the minimum mass is 2.09kg and the torque is 19.5Nm. Moreover, the power consumption  $P = 60.97W$  of this configuration is the least.

CONFIG	TB	TB0	MASS	PP	NTURN1
16	20.3816	0.145749	2.16623	65.5125	268.859
17	20.4959	0.146389	2.17445	65.6577	268.956
18	20.5635	0.14718	2.17663	63.3971	256.036
19	19.796	0.142079	2.11901	61.2022	249.223
20	19.6419	0.142795	2.09942	61.7672	252.212
21	19.7487	0.143803	2.10721	62.2215	253.763
22	19.6978	0.14569	2.10473	62.8988	256.062
23	20.1094	0.148456	2.13602	64.0382	259.493
24	20.2233	0.146992	2.14324	62.6343	252.601
25	20.106	0.146111	2.13471	62.2061	251.111
26	20.0363	0.146336	2.12821	62.4111	252.221
27	20.1306	0.147203	2.13515	62.7985	253.523
28	20.1541	0.149727	2.13956	63.953	257.79
29	19.4992	0.145125	2.08945	61.9735	251.605
30	19.5169	0.142822	2.0891	60.4339	244.824
31	19.8696	0.145267	2.1156	61.4615	248.041
32	19.9635	0.147184	2.12195	62.3561	251.332
33	19.8586	0.146646	2.11413	62.132	250.688
34	19.7829	0.145383	2.10815	61.4373	247.939
35	19.8474	0.145756	2.11303	61.5757	248.3
36	19.4977	0.143388	2.08669	60.5653	245.147
37	19.582	0.144774	2.09278	61.1904	247.409
38	19.4957	0.144269	2.0863	60.9754	246.759
39	19.426	0.141918	2.08376	59.6211	240.889
40	19.8844	0.14508	2.11773	60.9551	245.103

Figure 3.19 MRB optimal results.

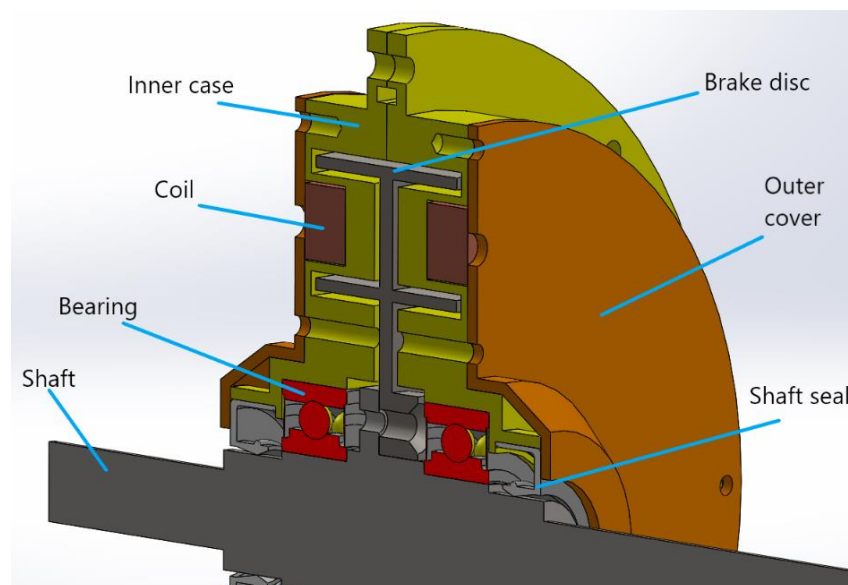
### ❖ Detailed design

During the assembly of the previous version of the I-shaped brake, a few problems were discovered. The first issue is that the shaft pad scrapes against the shaft seals of the inner case. Next are the threaded holes in the two parts of the housings that do not match, making it difficult to install screws. Finally, holes are required to properly insert the MRF into the brake.

This leads to vital requirements for the design:

- Fix the disc and shaft to avoid contacting the inner case.
- Install two bearings inside the case to avoid looseness when rotating.
- Do not allow the MRF to be leaked.

From the optimal results along with ensuring the above requirements, a prototype of the new MRB is designed to serve the experimental process. Based on Figure 3.20, the coil is wrapped around the groove which is considered the spool of the case. On the other hand, the two bearings on either side are responsible for keeping the case and disc a fixed gap to fill MRF in. The two sides of the case and the outer cover are attached with screws. Likewise, the shaft and disc are also connected by screws. The brake assembly procedure as well as the technical drawing are described in more detail in the section 'Computer-aided design 3D model'.



*Figure 3.20 Structure of new I-shaped MRB.*

### ❖ Attachment of MRB

- **Bearing:** SKF 6003-2RSH is chosen for this MRB because it not only keeps the disc rotating smoothly but also can prevent the MRF leaking out by two covers on both sides. Additionally, this bearing offers a reasonable price and easy to find at retail mechanics stores. It has technical parameter:

Bore diameter	$d = 17\text{mm}$
Outer diameter	$D = 35\text{mm}$
Width	$B = 10\text{mm}$
Limited speed	13000 r/min

- **Radial shaft seal:** SKF 15x28x7-CRW1-R is specialized in preventing the liquid from spilling out when the shaft is rotating.

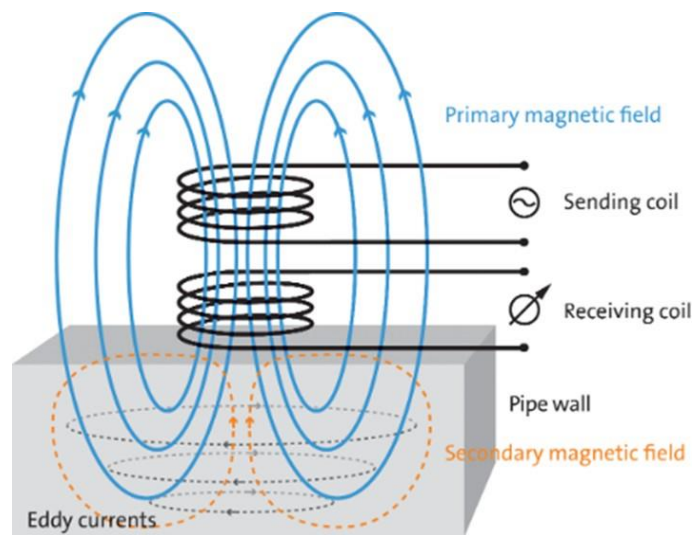
Shaft diameter	$d_1 = 15\text{mm}$
Pillar diameter	$D = 28\text{mm}$
Width	$b = 7\text{mm}$
Limited speed	3780 r/min
Operating temperature	min. $-40\text{ }^\circ\text{C}$ , max. $100\text{ }^\circ\text{C}$

### 3.3.3 Steering torque sensor

This thesis needs to use a torque sensor to measure the actual rotational force of the MR brake when experimenting. There are two types of dynamic torque sensors: torque sensors and non-contact torque sensors. More specifically, torque sensors are commonly used in spindle applications where accuracy is not required, while non-contact torque sensors provide accurate measurements at a high rotational speed. Because of the high accuracy, the contactless torque sensor is used in the ESP steering system or testing as the one this project needs.

These non-contact torque sensors work on the principle of eddy current. The sensor consists of two cylindrical coils: the primary coil (sending coil) and the secondary coil (receiving coil). When an alternating current travels through the coil, it creates a primary magnetic field. This magnetic field then generates eddy currents in the testing

target. The phase difference will be measured by comparison with the secondary coil and can be displayed on the screen.



*Figure 3.21 Eddy-current sensor [26].*

The structure of the eddy-current torque sensor is very complicated, but the simplification can be described in the figure below. The slot sleeves on the shaft are made of conductive metal and also the target where the eddy current appears. Electrical information is sensed in the secondary coil when the coil is energized and the shaft rotates. Then there will be a circuit to handle the amplitude-detecting circuit and output the signal.

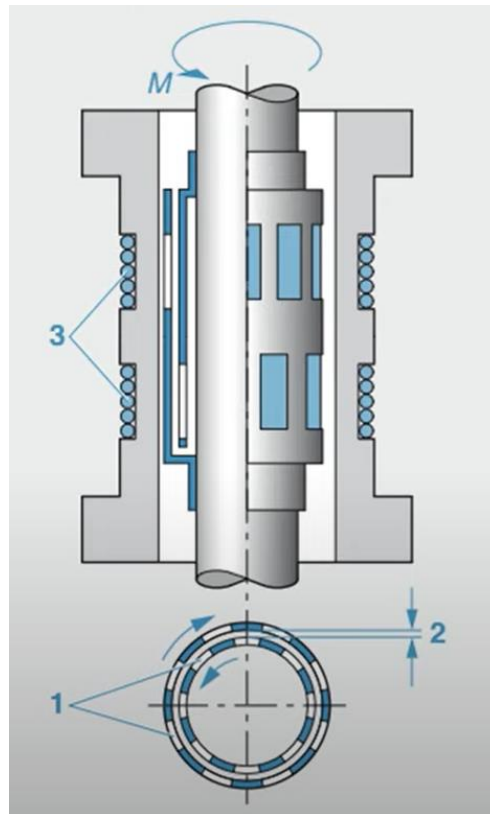



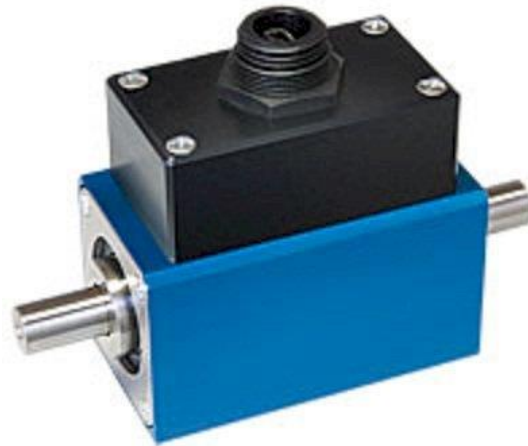
Figure 3.22 Eddy-current torque sensor [27].

- 
  
 1. Slotted sleeves  
 Vietnamese-German University  
 2. Air gap  
 3. High-frequency coils  
 M: Torque

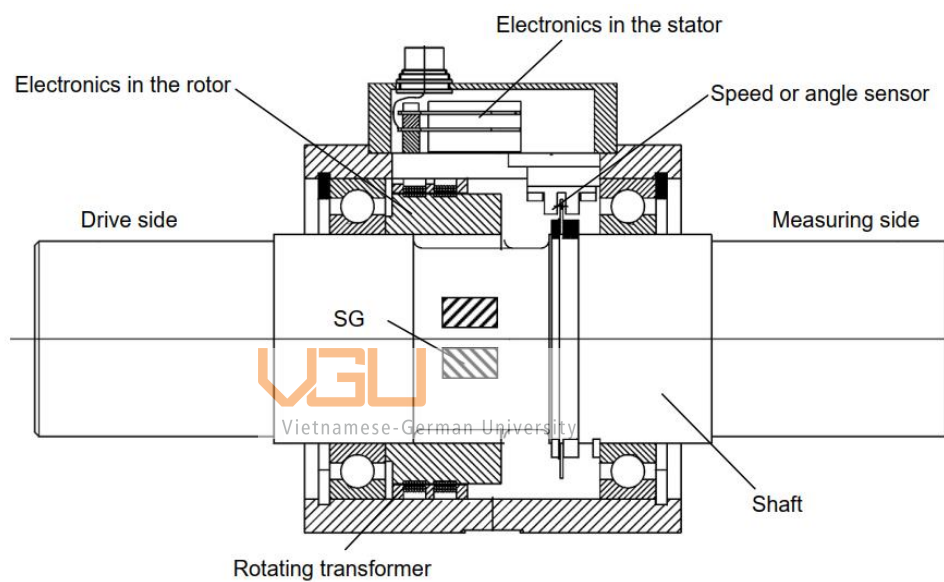
In this steering system, some conditions need to be considered such as:

- The non-contact transmission torque sensor is necessary to minimize the error between measuring components when the instrument is in operation. It means an eddy-current torque sensor is essential.
- USB-Torque sensor with configuration and evaluation software.
- Stable operation in dusty, and oily environments.
- Digital signal transmission from the rotor to the stator to avoid information interference.

To meet the above conditions, the rotary torque sensor DR-3000 from Lorenz-Messtechnik offer is the most suitable choice.



a)



b)

Figure 3.23 a) Torque sensor DR-3000 and b) its structure [28].

A circular transformer is made up of two symmetrically arranged coils. There is an air gap between the two coils. This allows one coil to be attached to the spindle and the other to be attached to the stator. Energy, or measurement signals, are transmitted in the same way that a transformer does. The spinning transformer's fixed portion and electronics are contained in the housing. A connector is placed in the enclosure for a power source of the sensor.

TTL signals are not generated by the sensor. It immediately outputs the conditioned angle signal in 1/4-degree increments. In the stator, the data signal is conditioned before



being transformed into a sequence output in a CPU. A converter converts every terminal data into USB communication. The data is then sent to a PC via a USB. According to the manufacturer, one should install the device mechanically during the installation at low torques (20 Nm) and evaluate the data; the evaluation output may not approach the specified torque.

### 3.3.4 Position steering sensor

An electromechanical detector that creates an electronic signal due to movement is known as an encoder. This device converts movement into a binary code or pulse using electromechanical means. The encoder is meant for determining the angular displacement of a revolving cylinder, such as a wheel disc, a camshaft, or any other unit that requires rotation position determination.

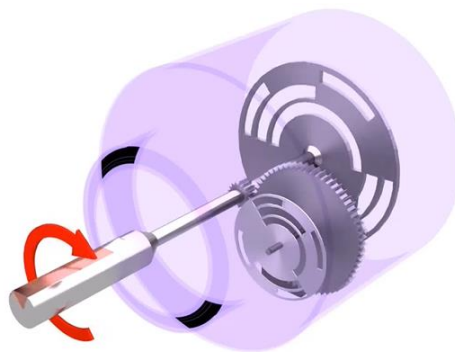
An encoder is often categorized solely on its own output methods, which are divided into two types: the absolute encoder and the incremental encoder.

#### ❖ Absolute encoder:



Vietnamese-German University

The transmitted input from the encoder is termed "absolute" because it signifies the precise position of the encoder even without customer needing to interpret anything more than that.



*Figure 3.24 Absolute encoder [29].*

- **Characteristics:**

- Utilize plate in either digital or grayscale mode.

- Consists of a light-emitting diode (LED), an engraver plate (with a decoding band), and often a light detector responding towards the light emission.
- The engraver plate is composed of hyaline material, and the plate surface is split into equal intervals by concentric rings.
- **Advantages:** If the encoder disconnects, the experimental value can still be retained.
- **Disadvantages:** Include high production costs as well as a complex and challenging signal.

❖ **Relative encoder (incremental encoder):**

Emits an incremental or cyclical signal with the help of two different phase tracks in detecting the rotation direction.



*Figure 3.25 Relative encoder [29].*

- **Characteristics:**
  - The encoder is comprised of a pulsed band that is generally split into different evenly spaced gaps.
  - Light may travel through the layer if it is translucent.
  - For an encoder with one, two, or three loops of slots, and frequently with an extra tracking slot.
- **Advantages:** low cost, simple fabrication, easy signal processing.
- **Disadvantage:** prone to pulse deviation when returning. Errors will accumulate with the long-term operation.

❖ **Conclusion:**

The encoder used in this thesis is OMRON E6B2-CWZ6C



*Figure 3.26 Encoder Omron E6B2-CWZ6C.*

• **Specifications:**

- Model: Omron E6B2-CWZ6C 1024 p/r
- Using voltage: 5~24VDC.
- Consumption current: max 80mA
- Number of pulses: 1024 pulses / 1 cycle (1024 p/r)
- Number of pulse channels: 3 separate pulse channels A, B, and Z.
- Maximum frequency response: 100Khz
- Pulse output type: NPN open collector (need to connect the resistor to VCC to make high level)
- Shaft diameter: 6mm
- Body diameter: 40mm

Table 9. Colors corresponding to the output.

Color	Output
Brown	VCC
Blue	OV
Ground wire	GND
Black	A
White	B
Orange	Z

### 3.4 Design and select steering components

#### 3.4.1 Shaft coupling

This system has many shafts that need to be linked together so shaft misalignment is inevitable. Furthermore, while the MR brake is in operation, vibration may also occur. Because of that, a flexible jaw coupling is a top priority. The proof is they typically accommodate angular shaft misalignment up to 1 degree and parallel misalignment up to 0.381mm.



  
*Figure 3.27 Flexible jaw coupling.*  
Vietnamese-German University

#### 3.4.2 Pillar block bearing

A pillow block bearing is an equipped bearing that supports the load on a spinning shaft. Pillow block bearings, also known as pedestal bearings, are housings with a bearing installed within. Because of that, the choice of bearing and pillow block bearing is equivalent. On the market today there are many industrial bearings designed with different characteristics. Each type will have its characteristics and uses. To find the right bearing, this thesis will rely on the most basic bearing selection criteria.

- **Operating condition**
  - Rotational speed:  $n = 50$  r/min
  - Shaft diameter: 25 mm
  - Angular velocity:  $\omega = n \times 2\pi/60 = 5.23$  rad/s
  - Mass of the shaft:  $G = 4$  kg
  - Operating temperature:  $T = 26$  °C (78.8 °F)

- Environment: the steering unit may be located indoors, laboratory with a cool air conditioner system, and a low dust environment.

- **Available space**

By the design, there is no space limitation. So, a shaft with a normal diameter can have any type of bearing width available.

- **Arrangement**

The shaft, like any other rotating device, is normally supported by a locating bearing and a non-locating bearing.

- The centering support determines the shaft's axial position about the housing.

- Non-locating bearings must be able to withstand axial movement of the shaft to avoid overloading. Bearing types suitable for use in the non-locating position include NU-type roller bearings, needle roller bearings, and N-type bearings.

- **Loads**

The magnitude of the load is an important factor in the selection of bearings. It is worth noting that under normal circumstances, the load capacity of a roller bearing will be higher than the ball bearing when the sizes of the two are similar. For this project, the load is very light as it only needs to bear the weight of the steering wheel about 2 kg, and the weight of the shaft less than 5 kg. A ball bearing is all it needed as a conclusion.

- **Precision**

The main grade of a bearing is another aspect that influences its selection. When working, we may think of the precision level as the dimension and tolerance level. The precision level of each bearing type is specified at the start of the specific parts for that bearing type.

- **Cost and availability**

After researching the market price and popularity of pillar block ball bearings, some of the most used ones that also have reasonable prices among the standard inner diameter 25 mm can be found as: UCF 205, KFL 205, P 205 and UCP 205.

- **Bearing size**

Based on a few basic parameters that different brands use in common to find the most suitable size product.

- Minimum load equation [30]:

$$F_{rm} = k_r \times \left(6 + \frac{4 \times n}{n_r}\right) \times \left(\frac{d_m}{100}\right)^2$$

Where  $F_{rm}$  minimum radial load [kN]

$k_r$  minimum load factor

$n$  rotational speed [r/min]

$n_r$  reference speed [r/min]

$d_m$  bearing mean diameter [mm]

With  $n = 100$  r/min,  $n_r = 4000$  r/min,  $d_m = 29.35$  mm. Then  $F_{rm} = 0.34$  kN

- Basic rating life equation [30]:



Vietnamese-German University

$$L_{10h} = \left(\frac{10^6}{60 \times n}\right) \times \left(\frac{C}{P}\right)^p$$

Where  $C$  dynamic load rating [kN]

$P$  dynamic bearing load [kN]

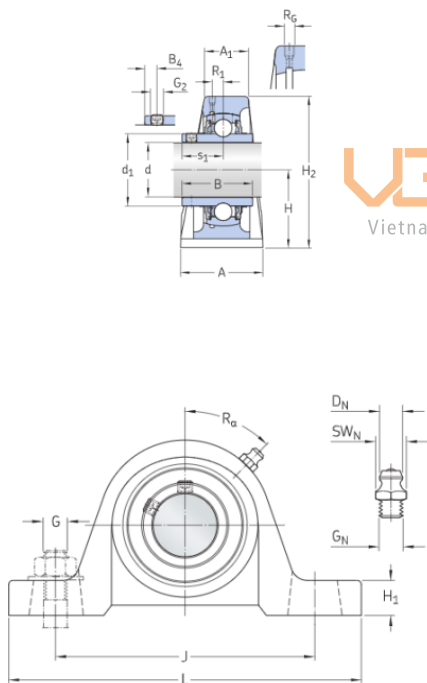
With  $P = 0.335$  kN, the load ratio  $C/P = 42$ . Then the basic rating life  $L_{10h} = 17520$  h, which means this bearing has a slightly longer life than the warranty period.

❖ **Conclusion:**

After an analysis, UCP 205 is the product the project is looking for that can meet the requirements mentioned above.



Figure 3.28 Pillow block ball bearing UCP 205 [31].



#### Dimensions

d	25 mm	Bore diameter
d <sub>1</sub>	≈ 33.7 mm	Shoulder diameter inner ring
A	38 mm	Base width
A <sub>1</sub>	23 mm	Top width
B	34 mm	Width of inner ring
B <sub>4</sub>	5.5 mm	Distance from locking device side face to thread centre
H	36.5 mm	Height of spherical seat centre
H <sub>1</sub>	16 mm	Foot height
H <sub>2</sub>	70.5 mm	Overall height
J	105 mm	Distance between attachment bolts
J	max. 110 mm	Distance between attachment bolts
J	min. 100 mm	Distance between attachment bolts
L	139.5 mm	Overall length
N	13 mm	Diameter of attachment bolt hole
N <sub>1</sub>	18 mm	Length of attachment bolt hole
s <sub>1</sub>	19.7 mm	Distance from locking device side face to raceway centre

Figure 3.29 UCP 205 technical specification provided by SKF [31].

### 3.4.3 Intermediate shaft

According to the design model shown in the Figure 3.23 below, the shaft acts as the actuator from the steering wheel to the torque sensor. In addition, the shaft needs to be fit in the UCP 205 pillar block bearing within the bore diameter 25mm. The intermediate shaft is made of steel C50 that has an allowable shear stress of  $\tau_{\text{allow}} = 400$  MPa [32]. The maximum torque applied to the shaft is the resistance torque MR brake create  $M = 20\text{Nm}$ . It is necessary to design the minimum diameter of the remaining portion of the shaft to withstand the required torque. Torsional shear stress equation for the outer radius circular shaft [33]:

$$\tau = \frac{M_T \times r}{I_T} \quad (11)$$

Where  $\tau$  is the shear stress [MPa]

$M_T$  is the torque applied to the shaft [Nm]

$I_T$  is the cross-section moment of inertia at polar

$r$  is the shaft radius [m]

For a solid shaft of radius  $r$ ,  $I_T = \frac{\pi \times r^4}{2} = \frac{\pi \times D^4}{32}$  with  $D$  is diameter

From equation (11):

$$400 \times 10^6 = \frac{20 \times (D/2)}{\frac{\pi D^4}{32}} \quad (12)$$

$$D = 9.28 \times 10^{-3} [m]$$

Round the number to 10mm for turning the intermediate shaft with a diameter that can be fitted with shaft coupling.

### 3.4.4 Steering wheel

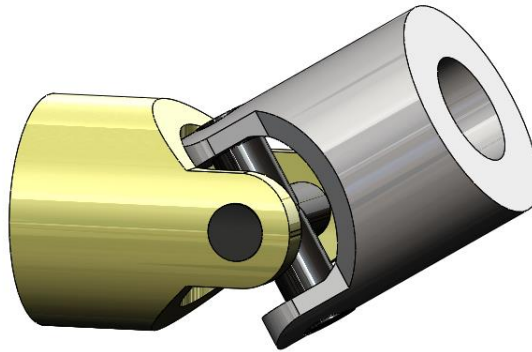
The common steering wheel diameter dimension on the market have the following standards:

- Size S: from 36cm usually fits small 4-seat cars.
- Size M: from 37.5 - 38cm, suitable for cars from 4 to 7 seats.
- Size L: from 39cm, suitable for cars from 7 to 16 seats.





conditions, the operation angle  $30^\circ$  is the optimal selection. Depending on the angle of rotation of the steering wheel, the rotation speed of the intermediate shaft and the steering column has a deviation of 10%. For the system, this deviation is accepted.



*Figure 3.31 Universal joint.*

#### ❖ Rotational position transmission

The requirement for the encoder is that it is not allowed to mount it directly on a shaft that is subjected to a torque load because the encoder shaft will be damaged. In order to transfer steering angle position information to the encoder, it needs to be indirectly through a mechanical transmission. The solution is using timing pulley and belt.



*Figure 3.32 Timing pulley set with belt.*

Timing pulley is different from regular pulley because it has teeth at the outer diameter similar to a gear. These teeth prevent pulley-belt misalignment and promote precise transmission. The pulley set selected in this system is XL type including two pulleys made of aluminum and one belt. Both pulleys are 30 teethed and have equal pitch. They differ in the dimension of the shaft diameter: 6mm is for the encoder shaft and 10mm is attached to the intermediate shaft.

### 3.5 Select power supply

Most other 220V electrical appliances have voltage converters to convert from alternating current (AC) to direct current (DC) or to lower voltages (from 3V to 60V) to power electronic components and semiconductors inside the machine. These electrical components often operate on very low DC voltages (ranging from 1.8V to 12V). As a result, DC power is an essential component for constructing electronic circuits, fixing electronic circuits, studying circuits, and developing microchips. Moreover, the DC power supply is also used in research and measurement in the laboratory.

There are two most common types of DC power sources:

#### ❖ Pulse power supply (honeycomb power supply)

There are fixed currents and voltages, for example, the output voltage is 3V or 5V or 12V, 24V, etc., and cannot be adjusted at will. These dc power supplies are most commonly found in desktops (PCs), printers, and laptops.



*Figure 3.33 Pulse power supply [34].*

- Advantages: Compact, lightweight, and cheap price.
- Disadvantages:
  - No display screen.
  - Cannot adjust the voltage.
  - The current is not high.

### ❖ DC power supply with variable output voltage

The normal voltage of this type of supply is usually adjustable from 0 ~ 60V, and the current can be selected from 0 ~ 20A.



Figure 3.34 Types of adjustable DC power supplies [35].

a) Switching power supply and b) Linear power supply

- Advantages:
  - For these supplies, there is adjustable output voltage as demand.
  - Large output current.
  - Display of voltage and current in use.
- Disadvantages: it is heavy, bulky, and has a high cost.

There are some demands for this thesis that needs to be considered:

- Output voltage: depending on the application that it can be from 0~120V.
- Power type: It is recommended to choose programmable DC power sources for high accuracy and stability.
- Resolution: from 1 $\mu$ V/1 $\mu$ A or less.
- Display: from 5~6 digits.
- There are communication ports: USB or GPIB.

- Switching or linear supply: linear supply usually has less ripple and side stability than switching sources, but the cost will be higher.

These programmable DC power supplies are usually only available from high-end US and European brands such as Tektronix, Keithley, Keysight, etc.

#### ❖ Conclusion:

In conclusion, with the help of VGU technicians in the electrical laboratory, this design project prefers the Keithley 2260B series with version 360W.

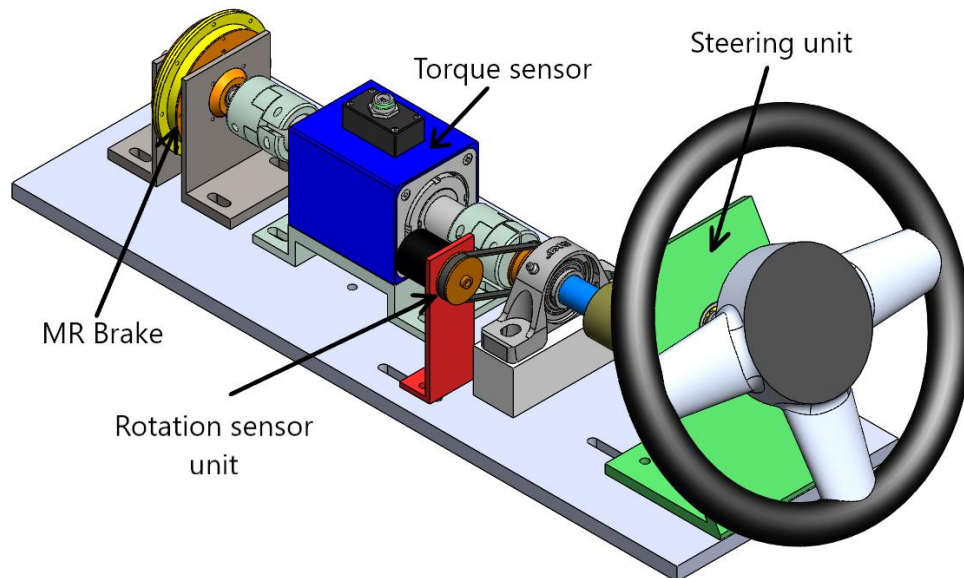


*Figure 3.35 Programmable DC power supply Keithley 2260B-80-13 [36].*

## 4. Computer-aided design section

### 4.1 Assembly overview

Figure 4.1 using isometric projection as a method visually demonstrating three-dimensional objects. Haptic feedback steering system is divided by groups to simplify the assembly process. The three main groups are MR brake, rotation sensor unit, and steering unit. Most of the parts are assembled together and with pedestals by screws. The assembly should pay attention to the equipment as well as the shafts must be concentric.



*Figure 4.1 Haptic feedback steering system 3D model*

#### **4.1.1 MRB assembly**

The assembly process is described in Figure 4.2 below. Firstly, the disc and brake shaft are attached together by four countersunk screws. Next, the two bearings slide on the shaft clamping to the ledge of the shaft. Then the two inner cases are assembled together and tightened with eight bolts and screws located at the rim. A radial shaft seal is inserted on the outside of the case to fit the shaft. Copper wire with a diameter of 0.5mm is wound into a coil with 200 turns. The coil is insulated to avoid contact with the case and placed in the bobbin slot. The two ends of the wire are put through a hole in the outer cover. Tighten the four screws that the arrow indicates to install the cover. Finally, inject MRF into the brake through the M3 threaded hole (refer to technical drawing Figure 4.9). After the installation of each component is completed, the MR brake is held in place on the system base by two brake holders.

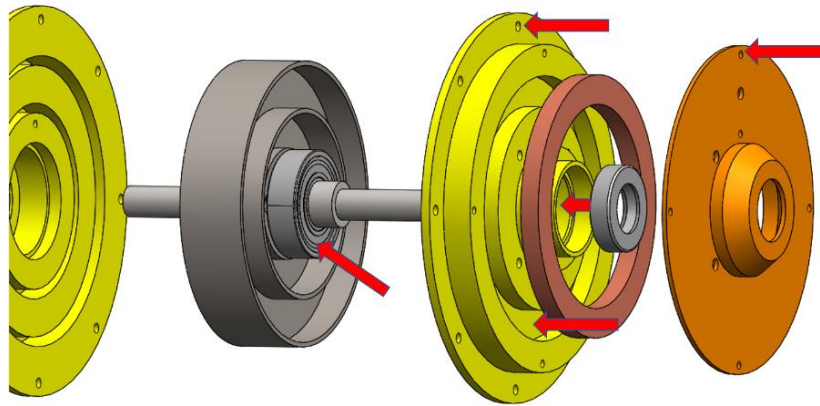


Figure 4.1 Exploded-view of MRB.

#### 4.1.2 Rotation sensor unit assembly

The first step is to install the torque sensor along with its pedestal to the system base. Furthermore, the torque sensor pedestal is pre-fabricated in VGU's laboratory. At the same time shaft coupling needs to be connected. In the second step, attach the encoder to a pedestal called the encoder holder. Then fix that holder to the system base. The next step is to install the toothed pulley with a bore diameter of 6mm to the encoder shaft. After fixing the pillar bearing pedestal, insert the intermediate shaft with a side diameter of 25mm into the pillar block bearing (as technical drawing Figure 4.12). The other side with a diameter of 10mm is fitted with a toothed pulley of the same bore diameter. Continuously, connect the toothed belt to the two pulleys and calibrate the position. Complete the installation by connecting the intermediate shaft and torque sensor shaft together and tightening all the screws.

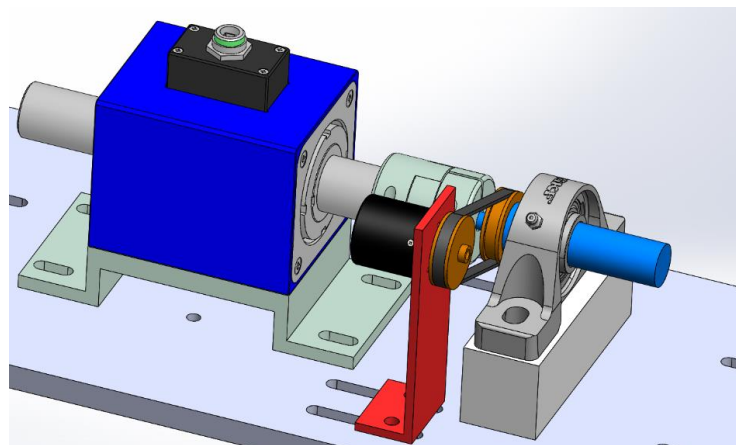


Figure 4.2 Rotation sensor unit.

### 4.1.3 Steering unit assembly

The assembly order is in the direction of the arrow (as shown in Figure 4.3). The steering pedestal is fixed to the system base with four screws. Bearing SKF 6005 with a bore diameter of 25mm is housed on the pedestal. Then put the steering column through the bearing. Next, attach the steering wheel to the column. Finally, attach the steering column to the universal joint.

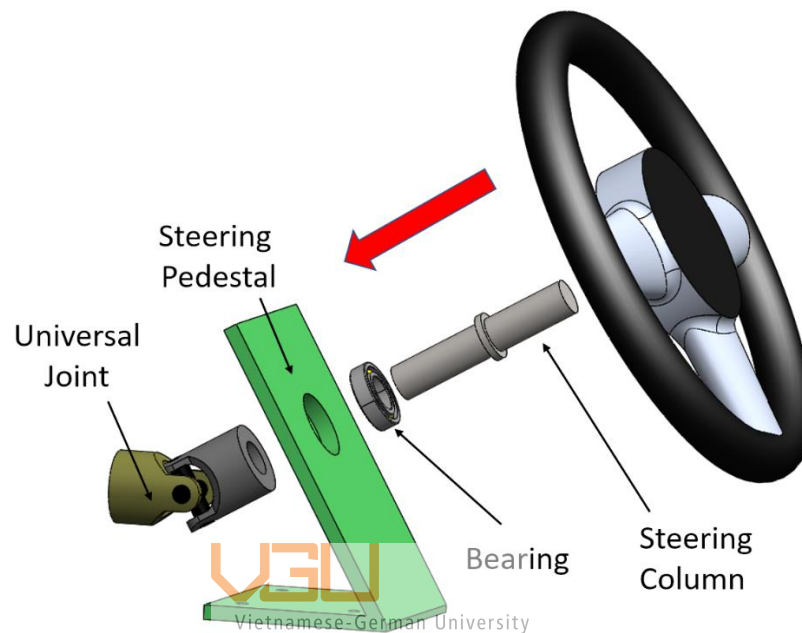


Figure 4.3 Exploded-view of steering unit.

### 4.2 Component technical drawing

The materials that are commonly used to machining parts:

- **Brake shaft:** stainless steel 304.
- **Brake disc:** steel C45.
- **Inner case:** steel C45.
- **Outer cover:** steel C45.
- **MRB holder:** aluminum A5052.
- **Bearing base:** cast iron.
- **Intermediate shaft:** steel C50.
- **Encoder holder:** aluminum A5052.
- **Steering column:** stainless steel 304.
- **Steering pedestal:** cast iron.
- **System base:** cast iron.



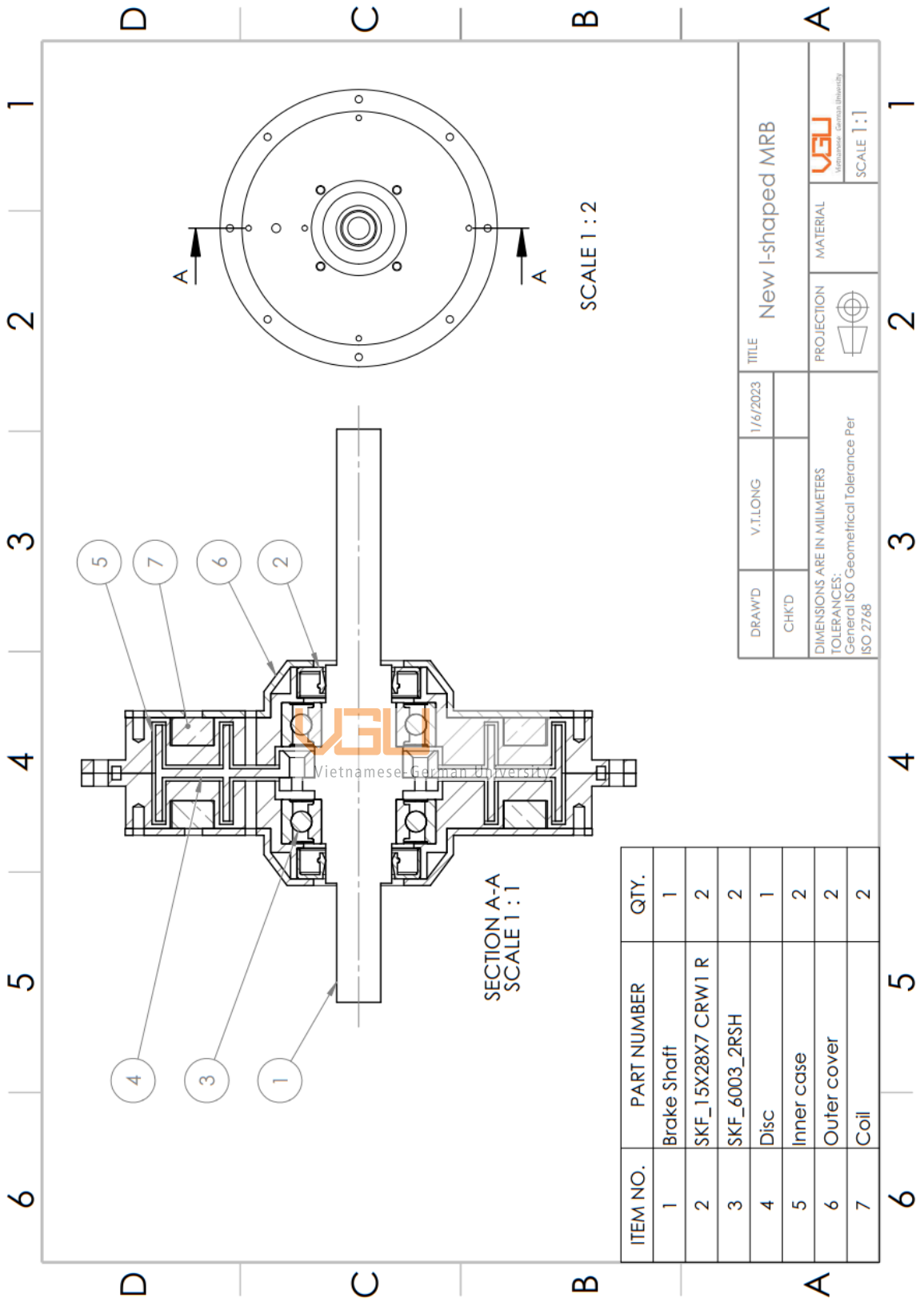


Figure 4.4 Technical drawing of MRB components.

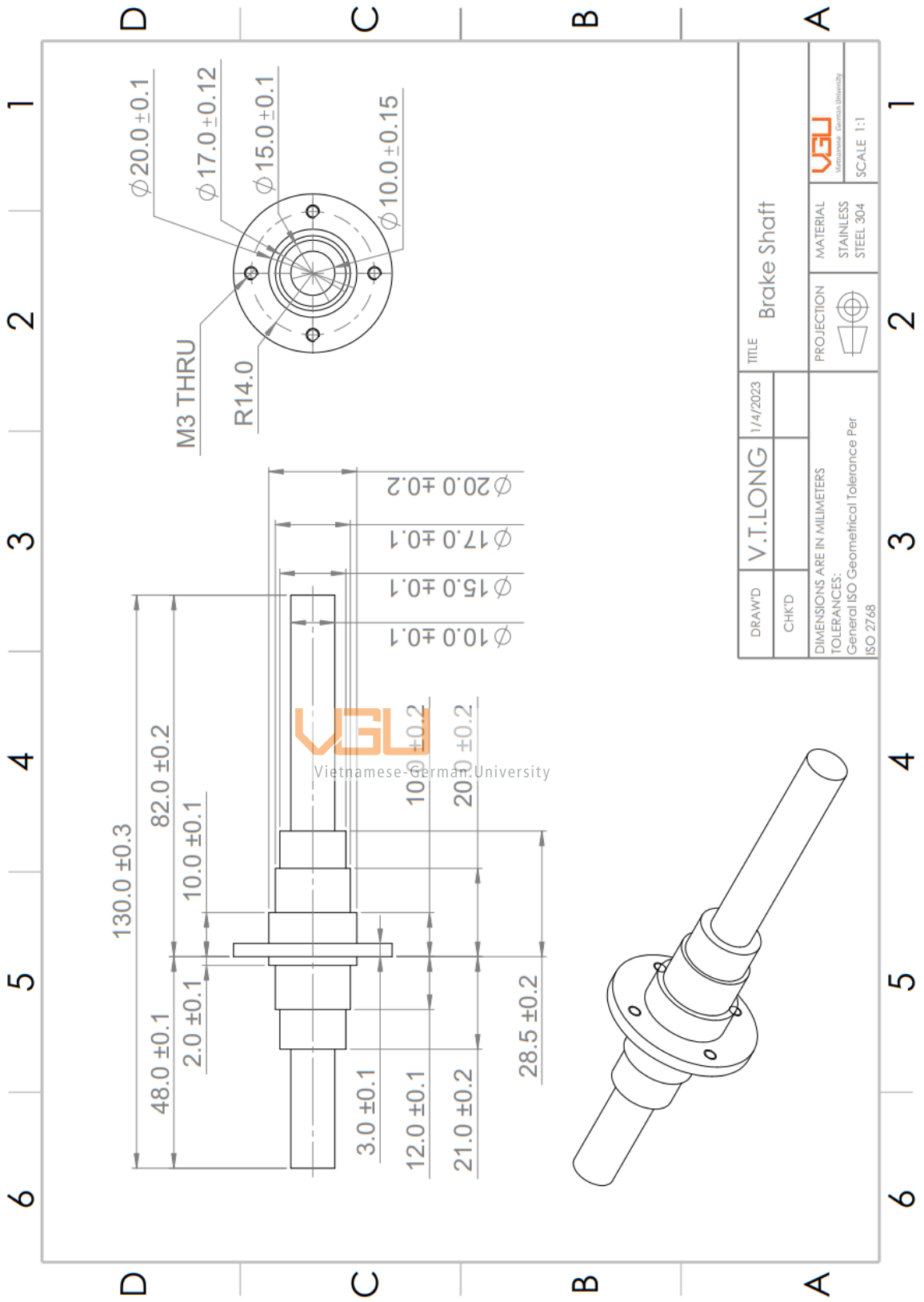


Figure 4.5 Technical drawing of brake shaft.



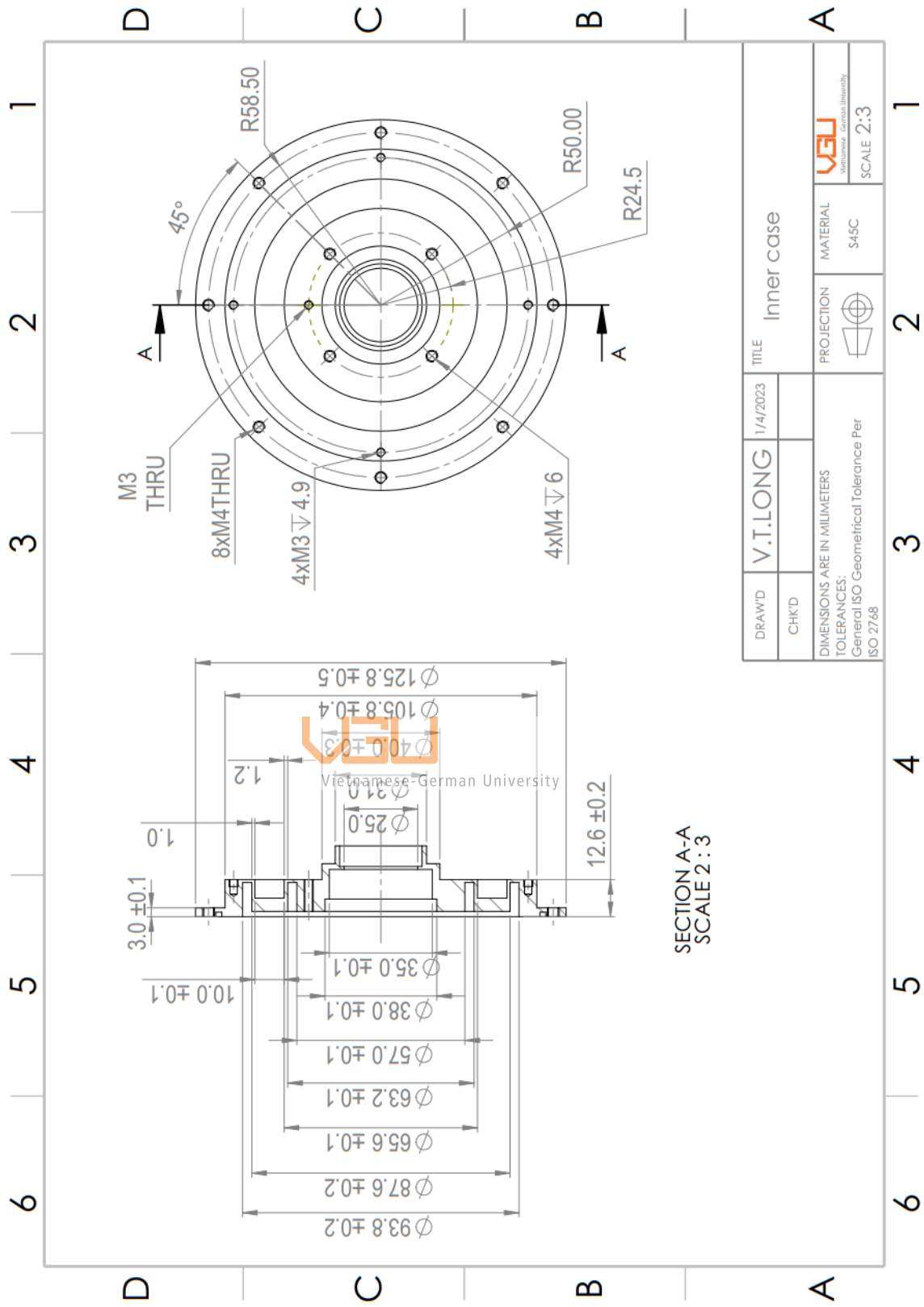


Figure 4.7 Technical drawing of inner case.

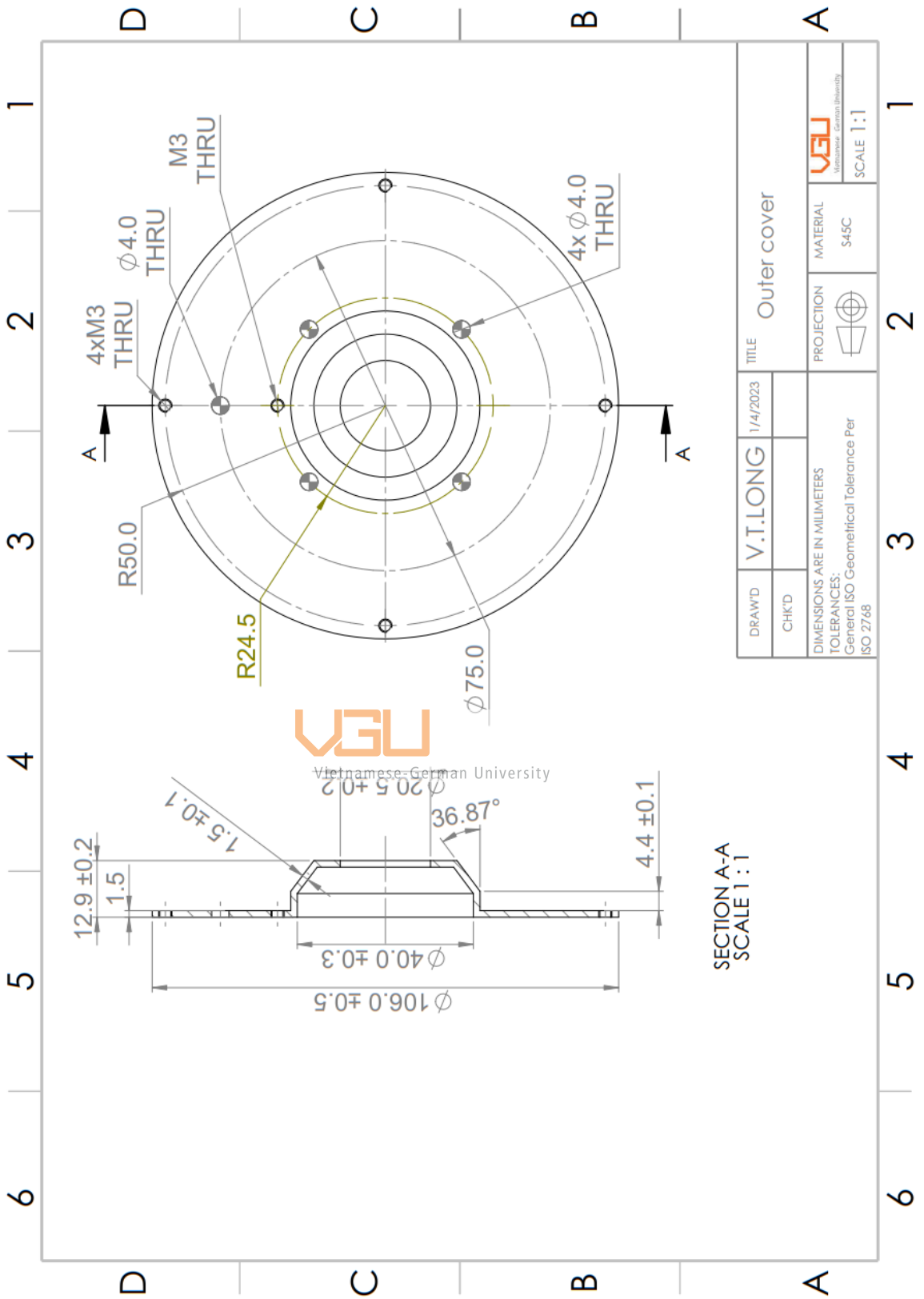


Figure 4.8 Technical drawing of outer cover.

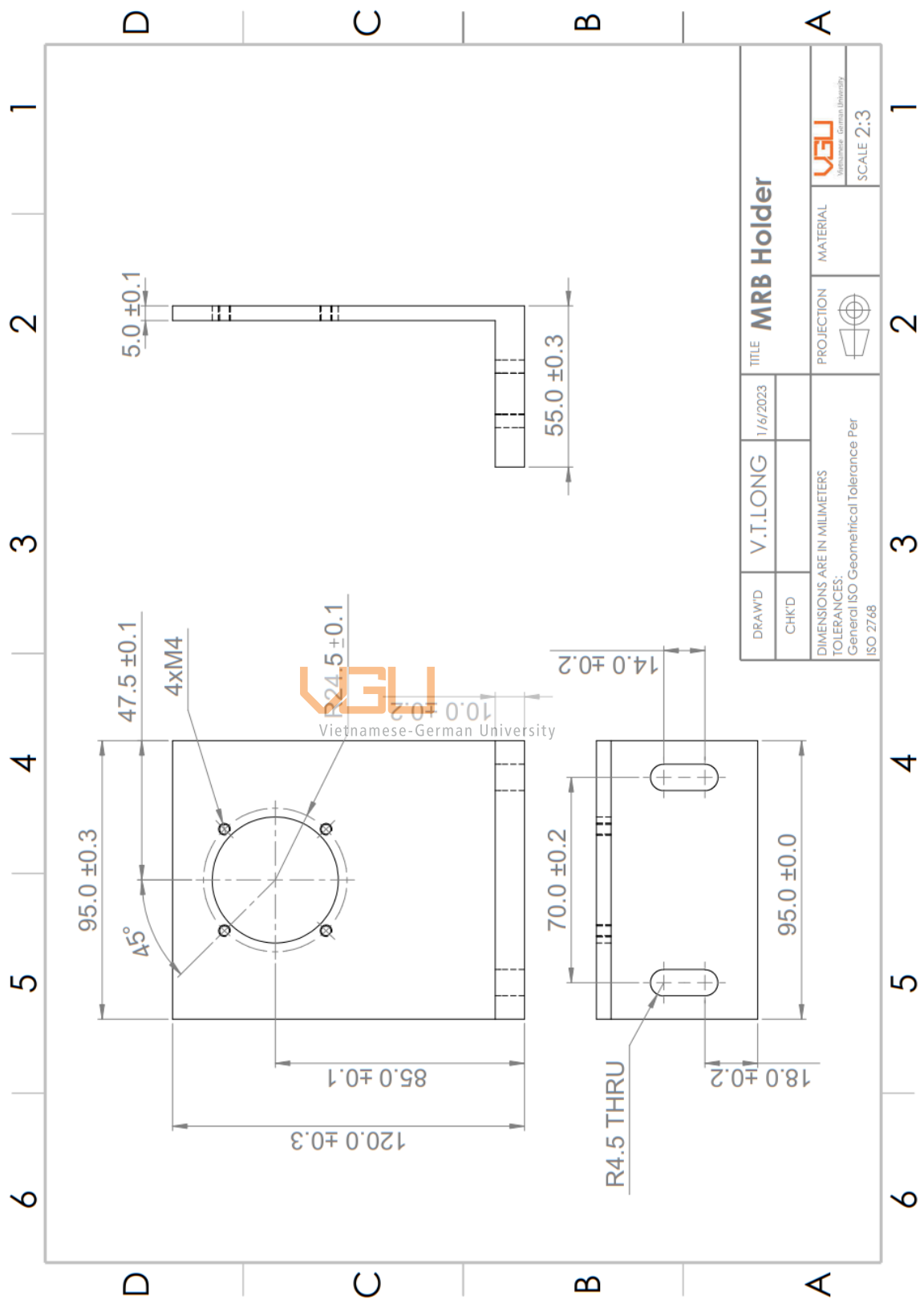


Figure 4.9 Technical drawing of MRB holder.

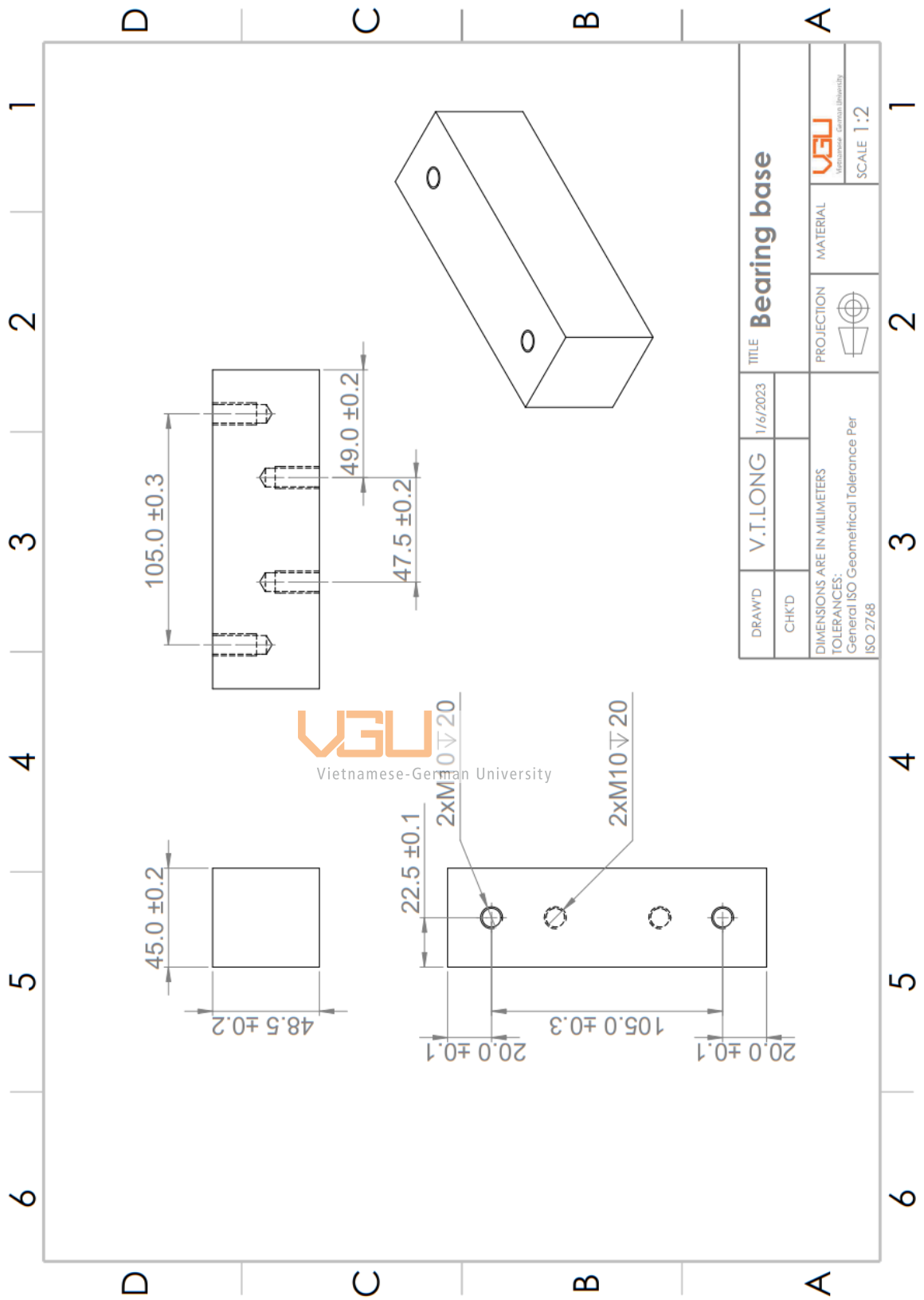


Figure 4.10 Technical drawing of bearing pillar base.

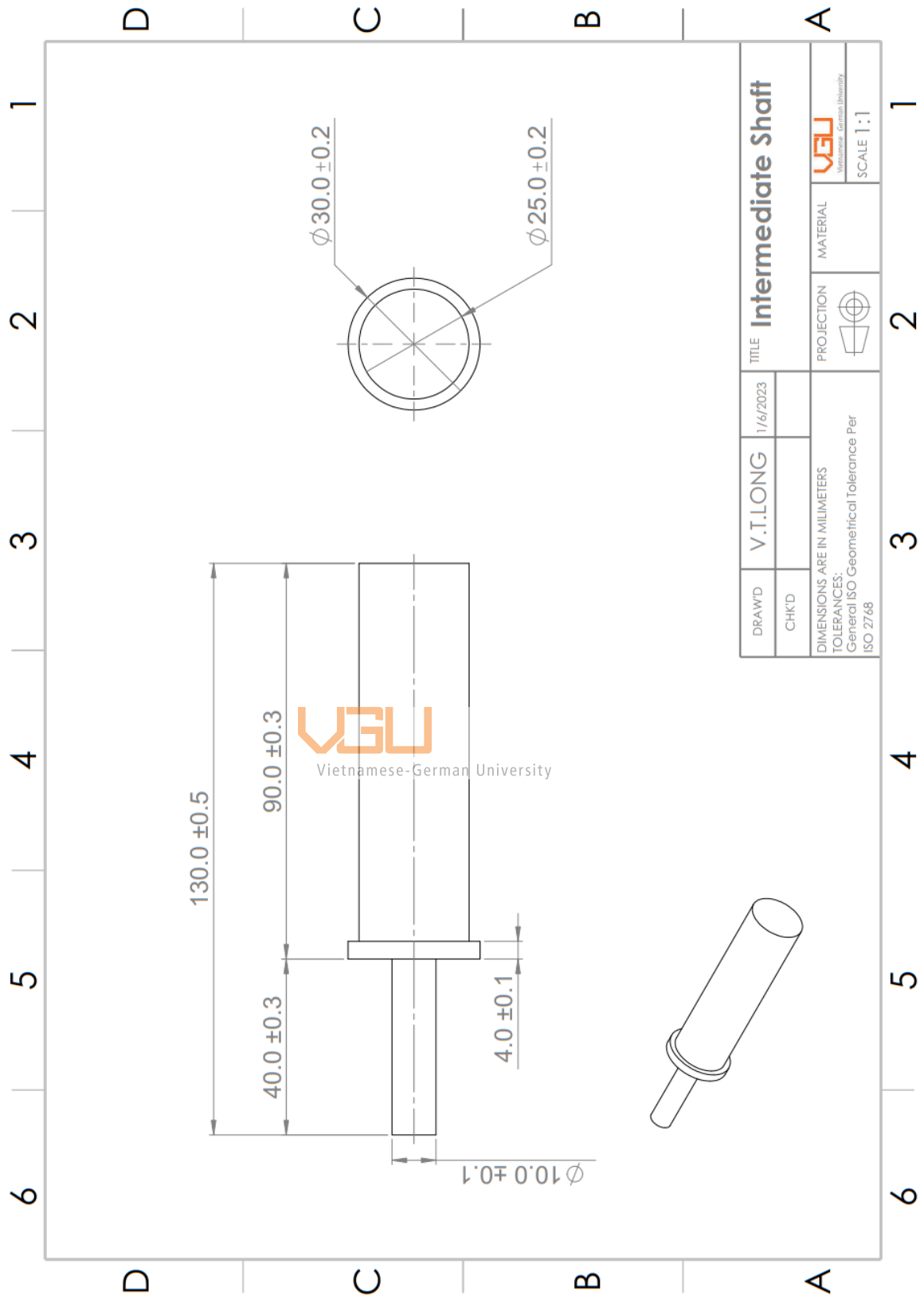


Figure 4.11 Technical drawing of intermediate shaft.



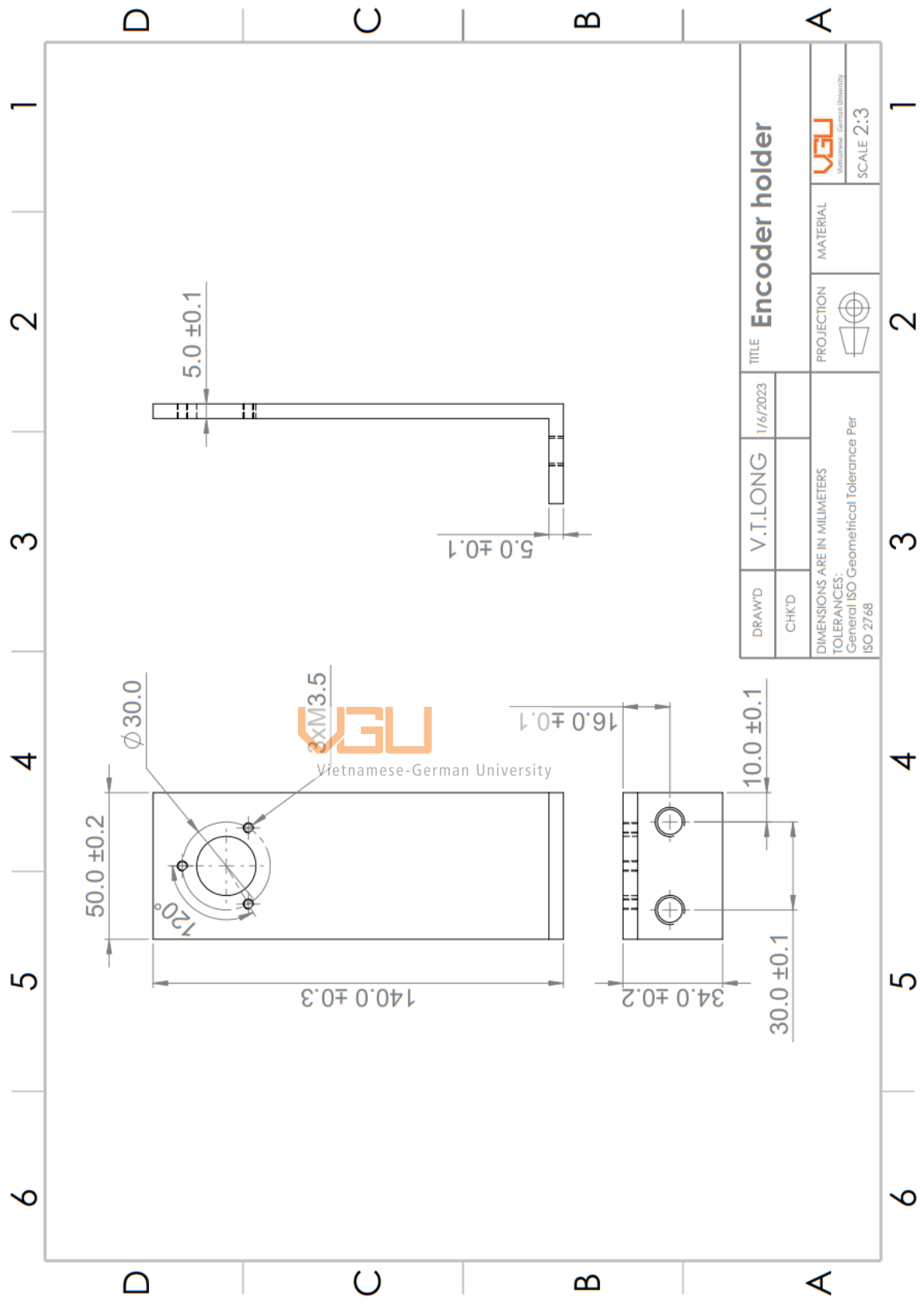


Figure 4.12 Technical drawing of encoder holder.

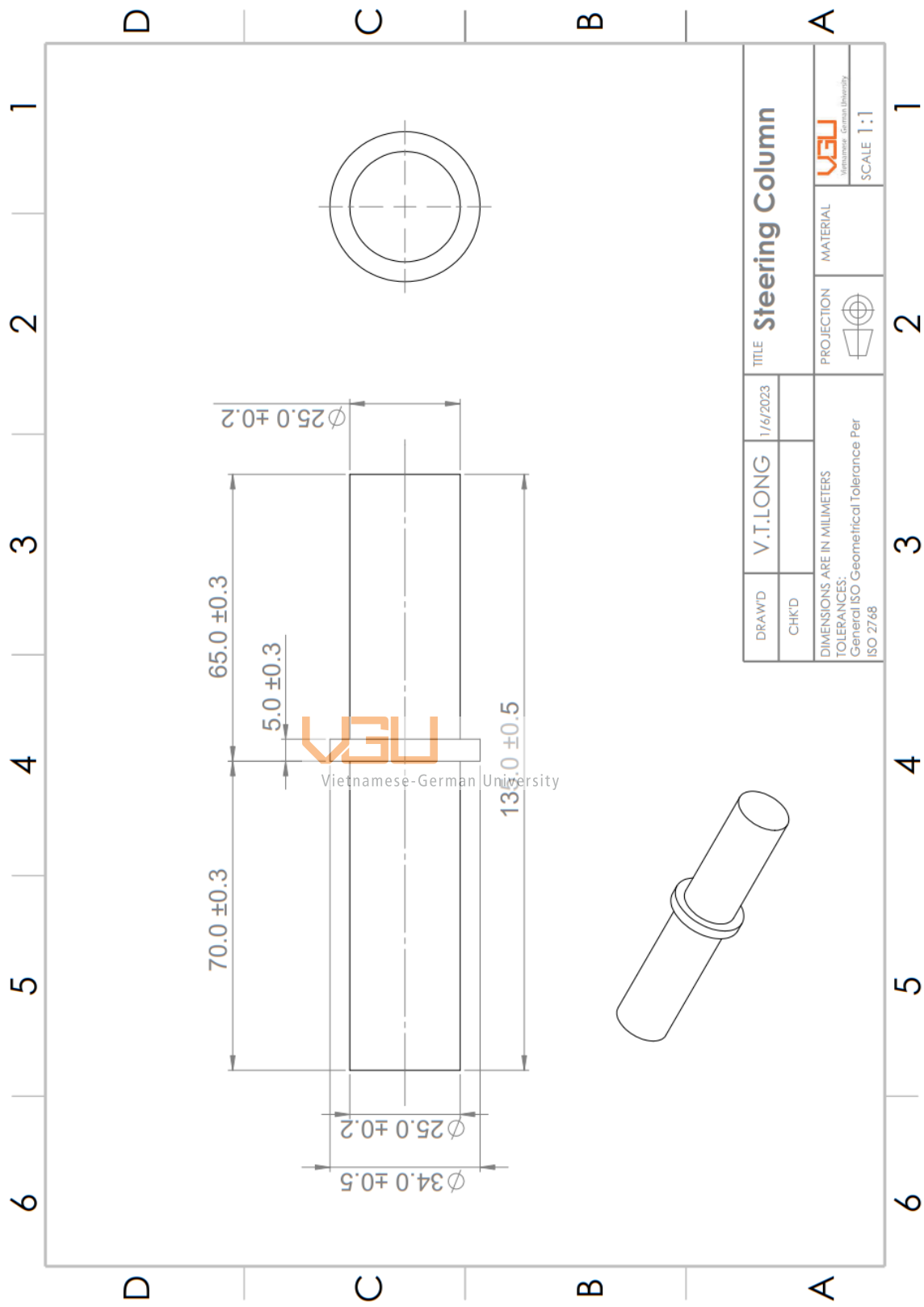


Figure 4.13 Technical drawing of steering column.

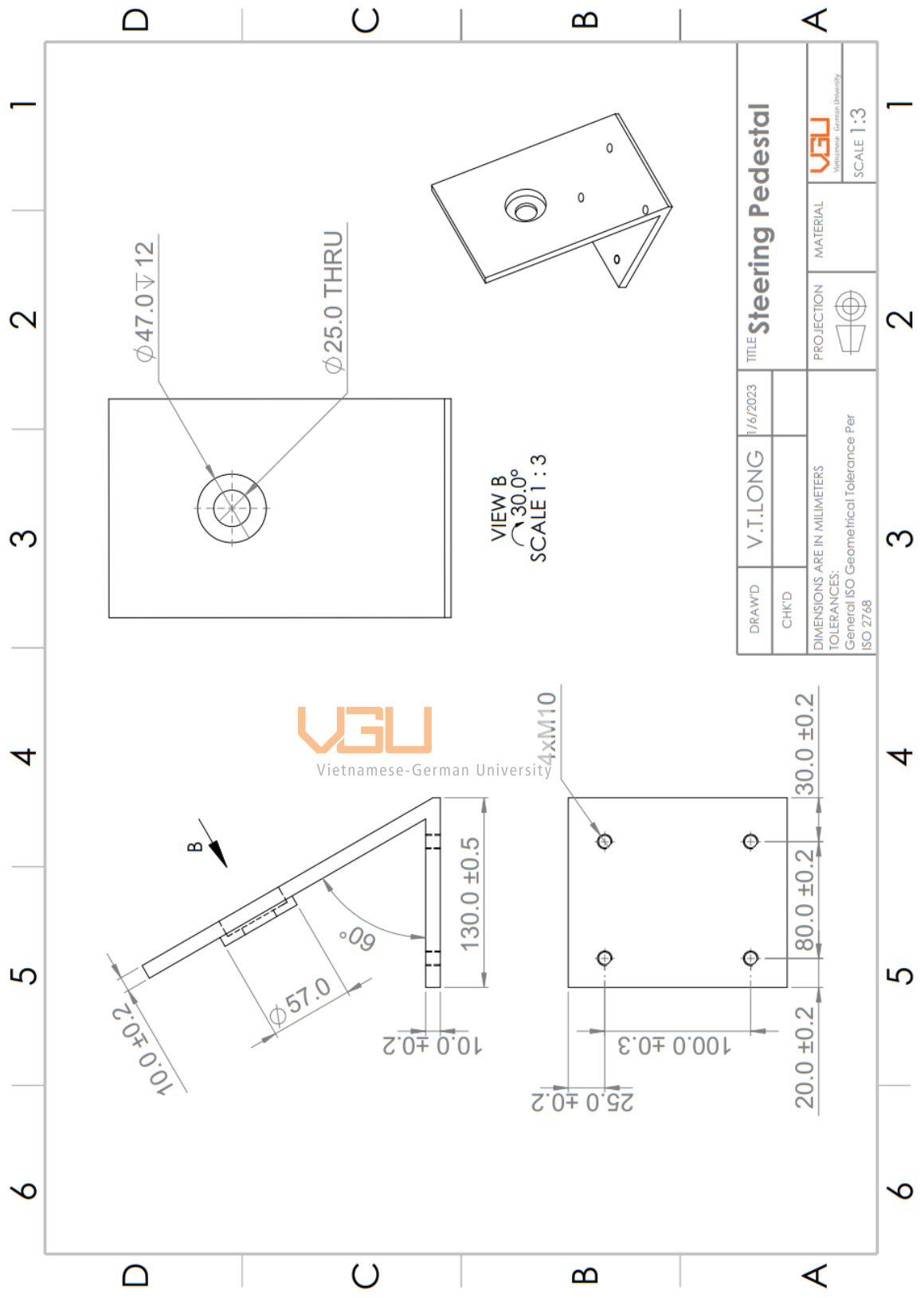


Figure 4.14 Technical drawing of steering pedestal.

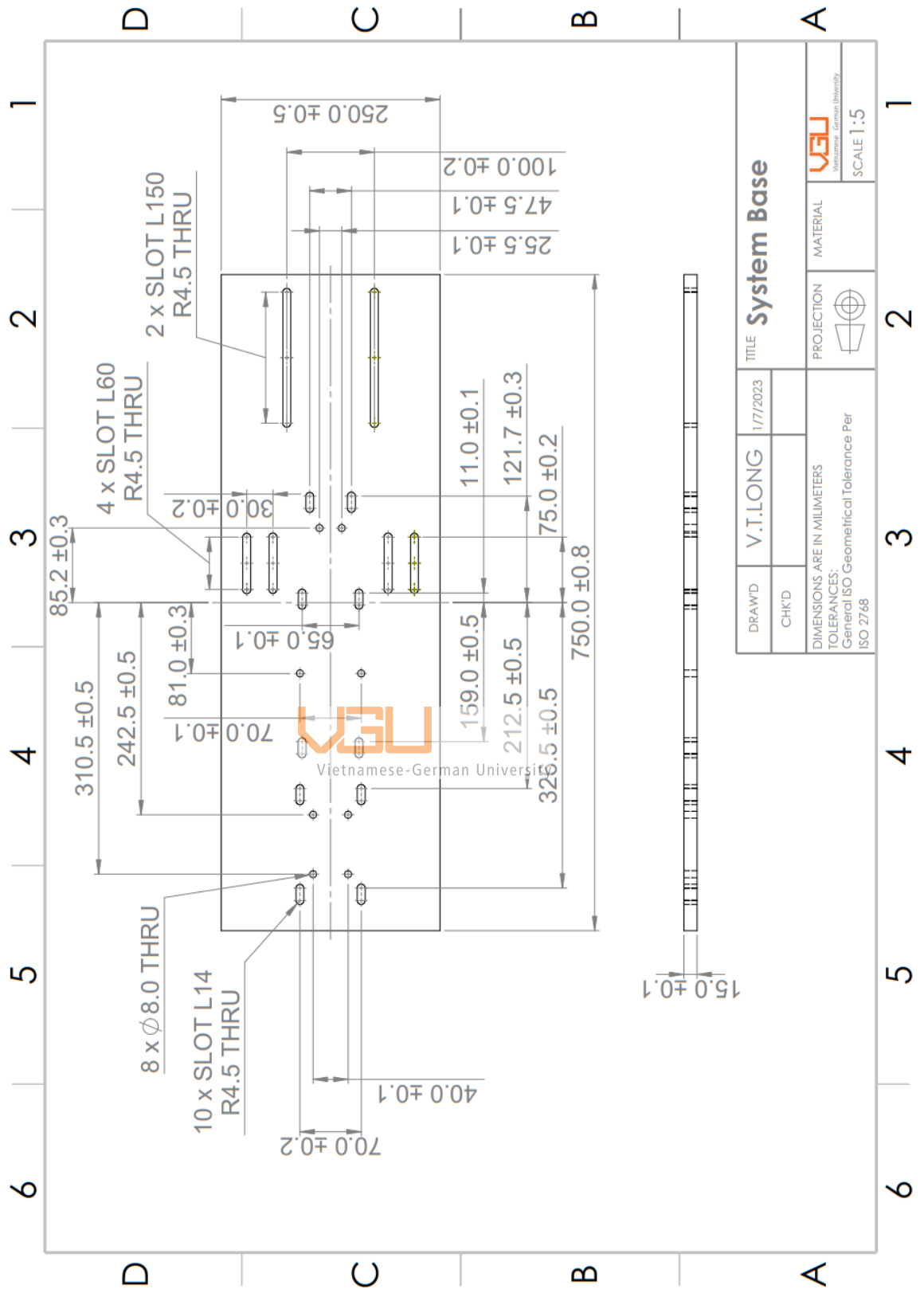


Figure 4.15 Technical drawing of system base.

## **5. Conclusion and future work**

### **5.1 Conclusion**

The final result of studying the topic of haptic feedback related to magnetorheological fluid is a simulation model that resembles reality. The improved design of the MR brake is based on experiences learned from previous prototypes. Both the brakes and the entire steering system met the computational requirements. 3D models in CAD and technical drawings help readers better understand the shape, structure, and operation of the system. However, some components, when calculated optimally in theory, will have difficulty in purchasing in practice. The design of a steering control system with haptic feedback requires a background of expertise in the field of electronic automation control, which is not the direction of this thesis study. Mechanical processing of a real model and testing this system in the laboratory is necessary.

### **5.2 Future work**

This model reinforces the practicality of researching a system that creates a driving sensation for the user. Furthermore, it plays a part in harnessing the potential of magnetorheological fluids. Hence, it needs improvements:

- Require programming software as well as electronic control circuitry.
- The alternate versions do not only stop at the brake, but could be innovated into more unique devices that associate with magnetorheological fluid.
- Design orientation to approach the low-end class vehicle in the future.

## REFERENCES

- [1] H. Team, “What Is Haptics? Part 1. Tactile Feedback,” *HaptX*, Nov. 08, 2017. <https://haptx.com/what-is-haptics-really/> (accessed May 31, 2022).
- [2] “What is a TFD® and How Does it Work?,” *LORD Corp*, May 15, 2018. <https://www.lord.com/products-and-solutions/steer-by-wire-tactile-feedback-device/what-is-a-tfd-and-how-does-it-work> (accessed Jun. 07, 2022).
- [3] “Haptic Technology: The Future of Engagement?” <https://masschallenge.org/article/haptic-technology> (accessed May 24, 2022).
- [4] J.-L. Aufranc (CNXSoft), “SmartKnob View is a DIY haptic input knob with WiFi and Bluetooth connectivity - CNX Software,” *CNX Software - Embedded Systems News*, Apr. 07, 2022. <https://www.cnx-software.com/2022/04/07/smartknob-view-is-a-diy-haptic-input-knob-with-wifi-and-bluetooth-connectivity/> (accessed Dec. 27, 2022).
- [5] V. Reports, “/PRNewswire/ -- The Haptic Technology Market is Segmented by Type (Tactile Feedback, Force Feedback), by Application (Automotive & Transportation, Consumer...” <https://www.prnewswire.com/news-releases/haptic-technology-market-size-to-reach-usd-25240-million-by-2027-at-cagr-14-5---valuates-reports-301381674.html> (accessed Jun. 10, 2022).
- [6] C. Pacchierotti, G. Salvietti, I. Hussain, L. Meli, and D. Prattichizzo, “The hRing: A wearable haptic device to avoid occlusions in hand tracking,” in *2016 IEEE Haptics Symposium (HAPTICS)*, Philadelphia, PA, USA, Apr. 2016, pp. 134–139. doi: 10.1109/HAPTICS.2016.7463167.
- [7] L. van den Bedem, R. Hendrix, N. Rosielle, M. Steinbuch, and H. Nijmeijer, “Design of a minimally invasive surgical teleoperated master-slave system with haptic feedback,” in *2009 International Conference on Mechatronics and Automation*, Changchun, China, Aug. 2009, pp. 60–65. doi: 10.1109/ICMA.2009.5246502.
- [8] “Amazon.com: Thrustmaster TX Racing Wheel Ferrari 458 Italia Edition (XBOX Series X/S, XOne & Windows) : Everything Else.” <https://www.amazon.com/Thrustmaster-Racing-Wheel-Ferrari-Italia-Windows/dp/B00ENFVS5Y?th=1> (accessed Dec. 23, 2022).
- [9] J. Wang and G. Meng, “Magnetorheological fluid devices: Principles, characteristics and applications in mechanical engineering,” *Proc. Inst. Mech. Eng. Part J. Mater. Des. Appl.*, vol. 215, no. 3, pp. 165–174, Jul. 2001, doi: 10.1243/1464420011545012.
- [10] M. Ashtiani, S. H. Hashemabadi, and A. Ghaffari, “A review on the magnetorheological fluid preparation and stabilization,” *J. Magn. Magn. Mater.*, vol. 374, pp. 716–730, Jan. 2015, doi: 10.1016/j.jmmm.2014.09.020.
- [11] O. Ashour, C. A. Rogers, and W. Kordonsky, “Magnetorheological Fluids: Materials, Characterization, and Devices,” *J. Intell. Mater. Syst. Struct.*, vol. 7, no. 2, pp. 123–130, Mar. 1996, doi: 10.1177/1045389X9600700201.
- [12] M. R. Jolly and J. D. Carlson, “Properties and Applications of Magnetorheological Fluids,” *Actuator 96 5th Int Conf New Actuators*, 1996.
- [13] Arus Mr Tech Private Limited, “AMT - SMARTEC ( Magnetorheological Fluid),” *indianmart*. <https://www.indiamart.com/falcon-mr-tech/magnetorheological-fluid.html>
- [14] J. S. Kumar, P. S. Paul, G. Raghunathan, and D. G. Alex, “A review of challenges and solutions in the preparation and use of magnetorheological fluids,” *Int. J.*

- Mech. Mater. Eng.*, vol. 14, no. 1, p. 13, Dec. 2019, doi: 10.1186/s40712-019-0109-2.
- [15] J. Huang, P. Wang, and G. Wang, “Squeezing Force of the Magnetorheological Fluid Isolating Damper for Centrifugal Fan in Nuclear Power Plant,” *Sci. Technol. Nucl. Install.*, vol. 2012, p. e175703, Oct. 2012, doi: 10.1155/2012/175703.
- [16] Y. H. Heo, D.-S. Choi, I.-H. Yun, and S.-Y. Kim, “A Tiny Haptic Knob Based on Magnetorheological Fluids,” *Appl. Sci.*, vol. 10, no. 15, Art. no. 15, Jan. 2020, doi: 10.3390/app1015118.
- [17] L. H. Hamdan, S. A. Mazlan, S. Sarip, H. Zamzuri, and M. A. A. Rahman, “Selection of Materials in Designing Magnetorheological Brake,” *Appl. Mech. Mater.*, vol. 663, pp. 700–704, Oct. 2014, doi: 10.4028/www.scientific.net/AMM.663.700.
- [18] Q. H. Nguyen and S. B. Choi, “Selection of magnetorheological brake types via optimal design considering maximum torque and constrained volume,” *Smart Mater. Struct.*, vol. 21, no. 1, p. 015012, Jan. 2012, doi: 10.1088/0964-1726/21/1/015012.
- [19] Q. H. Nguyen and S. B. Choi, “Optimal design of an automotive magnetorheological brake considering geometric dimensions and zero-field friction heat,” *Smart Mater. Struct.*, vol. 19, no. 11, p. 115024, Nov. 2010, doi: 10.1088/0964-1726/19/11/115024.
- [20] N. V. Bien, D. B. Tri, V. V. Bo, and N. Q. Hung, “Development of a Compact Size Magneto-Rheological Brake Featuring I-shaped Rotor,” in *Proceedings of the International Conference on Advanced Mechanical Engineering, Automation, and Sustainable Development 2021 (AMAS2021)*, B. T. Long, H. S. Kim, K. Ishizaki, N. D. Toan, I. A. Parinov, and Y.-H. Kim, Eds. Cham: Springer International Publishing, 2022, pp. 355–359. doi: 10.1007/978-3-030-99666-6\_53.
- [21] Quoc Hung Nguyen, V. B. Nguyen, H. D. Le, D. Q. Duyen, W. Li, and N. X. Hung, “Development of a novel magnetorheological brake with zigzag magnetic flux path,” *Smart Mater. Struct.*, vol. 30, no. 12, p. 125028, Dec. 2021, doi: 10.1088/1361-665X/ac3430.
- [22] S. Choi, “Design and Experimental Evaluation a novel magneto- rheological brake with toothed shaped rotor,” p. 28.
- [23] N. D. Nguyen, T. T. Nguyen, D. H. Le, and Q. H. Nguyen, “Design and investigation of a novel magnetorheological brake with coils directly placed on side housings using a separating thin wall,” *J. Intell. Mater. Syst. Struct.*, vol. 32, no. 14, pp. 1565–1579, Aug. 2021, doi: 10.1177/1045389X21993912.
- [24] “Toyota RAV4 Service Manual: Steering column assembly - Steering column.” [https://www.trav4.net/steering\\_column\\_assembly-1173.html](https://www.trav4.net/steering_column_assembly-1173.html) (accessed Dec. 29, 2022).
- [25] “Freightliner Century Coronado Columbia Upper Steering Column Cover,” *Raney’s Truck Parts*. <https://www.raneystruckparts.com/freightliner-century-coronado-columbia-upper-steering-column-cover/> (accessed Dec. 29, 2022).
- [26] “What is the difference between variable reluctance and eddy current speed sensors?” <https://www.sensortips.com/featured/what-is-the-difference-between-variable-reluctance-and-eddy-current-speed-sensors/> (accessed Dec. 29, 2022).
- [27] “sensors\_i-business.pdf.” Accessed: Dec. 29, 2022. [Online]. Available: [https://www.bosch-ibusiness.com/media/images/products/sensors/xx\\_pdfs\\_1/sensors\\_i-business.pdf](https://www.bosch-ibusiness.com/media/images/products/sensors/xx_pdfs_1/sensors_i-business.pdf)

- [28] “USB Torque Sensor, Rotating, Contactless DR-3000.” [https://www.lorenz-messtechnik.de/english/products/rotating\\_contactless/dr-3000.php](https://www.lorenz-messtechnik.de/english/products/rotating_contactless/dr-3000.php) (accessed Dec. 29, 2022).
- [29] *Engineering simulation film – Absolute encoder function*, (2017). Accessed: Dec. 29, 2022. [Online Video]. Available: [https://www.youtube.com/watch?v=yOmYCh\\_i\\_JI](https://www.youtube.com/watch?v=yOmYCh_i_JI)
- [30] “Loads | SKF.” <https://www.skf.com/group/products/rolling-bearings/engineered-products/hybrid-bearings/loads> (accessed Jan. 10, 2023).
- [31] “UCP 205 - Ball bearing units | SKF.” <https://www.skf.com/group/products/mounted-bearings/ball-bearing-units/pillow-block-ball-bearing-units/productid-UCP%20205> (accessed Nov. 30, 2022).
- [32] “EN 1.0540 (C50) Non-Alloy Steel :: MakeItFrom.com.” <https://www.makeitfrom.com/material-properties/EN-1.0540-C50-Non-Alloy-Steel> (accessed Jan. 10, 2023).
- [33] D. Gross, W. Ehlers, P. Wriggers, J. Schröder, and R. Müller, *Mechanics of Materials – Formulas and Problems*. Berlin, Heidelberg: Springer Berlin Heidelberg, 2017. doi: 10.1007/978-3-662-53880-7.
- [34] “Honeycomb Power Supply 5V 15A PSU - Brand New and Working Condition (LAST 2 SETS),” *Carousell*. <https://www.carousell.sg/p/honeycomb-power-supply-5v-15a-psu-brand-new-and-working-condition-last-2-sets-1068256940/> (accessed Dec. 29, 2022).
- [35] “DC Power Supply, 30V 5A Adjustable Switching Regulated DC Bench Linear Power Supply with Alligator Leads and 3 LED Digital Display, Variable Power Supply with US 3-Prong Cable | Fado.” <https://fado.vn/us/amazon/drmeter-dc-power-supply-30v-5a-adjustable-switching-regulated-dc-bench-linear-power-supply-with-alligator-leads-and-3-led-digital-display-variable-power-supply-with-us-3-prong-cable-B00O8DJ8QC.html> (accessed Dec. 29, 2022).
- [36] “Keithley 2260B-80-13 Programmable DC Power Supplies (80V, 13A, 360W).” [https://emin.vn/en\\_US/keithley2260b-80-13-keithley-2260b-80-13-programmable-dc-power-supplies-80v-13a-360w-9200/pr.html](https://emin.vn/en_US/keithley2260b-80-13-keithley-2260b-80-13-programmable-dc-power-supplies-80v-13a-360w-9200/pr.html) (accessed Dec. 29, 2022).



## APPENDIX

### Reference price list of items

Name	Qty.	Price (vnd)
SKF 6003-2RSH	2	220.000
SKF 15x28x7-CRW1-R	2	350.000
Copper wire coil	2	200.000
SKF UCP-205	1	250.000
SKF 6005	1	135.000